NAVAL POSTGRADUATE SCHOOL

MONTEREY, CALIFORNIA

THESIS

MODELING AND SIMULATION OF THREE-PHASE AC MICROGRID

by

Charles Y. Hirsch

March 2020

Thesis Advisor: Giovanna Oriti
Co-Advisor: Roberto Cristi

THIS PAGE INTENTIONALLY LEFT BLANK

REPORT DOCUMENTATION PAGE			*Form Approved OMB No. 0704-0188*

1. AGENCY USE ONLY ***(Leave blank)***	**2. REPORT DATE** March 2020	**3. REPORT TYPE AND DATES COVERED** Master's thesis

4. TITLE AND SUBTITLE MODELING AND SIMULATION OF THREE-PHASE AC MICROGRID	**5. FUNDING NUMBERS**
6. AUTHOR(S) Charles Y. Hirsch	
7. PERFORMING ORGANIZATION NAME(S) AND ADDRESS(ES) Naval Postgraduate School Monterey, CA 93943-5000	**8. PERFORMING ORGANIZATION REPORT NUMBER**
9. SPONSORING / MONITORING AGENCY NAME(S) AND ADDRESS(ES) N/A	**10. SPONSORING / MONITORING AGENCY REPORT NUMBER**

11. SUPPLEMENTARY NOTES The views expressed in this thesis are those of the author and do not reflect the official policy or position of the Department of Defense or the U.S. Government.

12a. DISTRIBUTION / AVAILABILITY STATEMENT Approved for public release. Distribution is unlimited.	**12b. DISTRIBUTION CODE** A

13. ABSTRACT (maximum 200 words)

Sustainable power at the forefront of Department of Defense operations is paramount on the battlefield as well as at naval installations around the world, and microgrid technology enables the deployment of renewable energy sources. This thesis develops a physics-based model of a three-phase microgrid set up with three commercial-off-the-shelf (COTS) inverters and a battery bank as its energy storage system. Both the model and the laboratory microgrid can be operated in grid-tied or in islanding mode. The microgrid's voltage waveforms, spectra, total harmonic distortion, and current waveforms are predicted by simulations and measured in the laboratory. IEEE Standard 519 and the manufacturer's performance standards provide the metrics for the power quality analysis. Comparisons of performance of the model to experimental laboratory data determine that the COTS units conform to IEEE Standard 519 and are suitable for further studies into microgrid expansion, management, and employment.

14. SUBJECT TERMS microgrid, three phase power system, microgrid control systems, photovoltaic power source, battery charge/discharge, island mode	**15. NUMBER OF PAGES** 75
	16. PRICE CODE

17. SECURITY CLASSIFICATION OF REPORT Unclassified	**18. SECURITY CLASSIFICATION OF THIS PAGE** Unclassified	**19. SECURITY CLASSIFICATION OF ABSTRACT** Unclassified	**20. LIMITATION OF ABSTRACT** UU

NSN 7540-01-280-5500 Standard Form 298 (Rev. 2-89) Prescribed by ANSI Std. 239-18

THIS PAGE INTENTIONALLY LEFT BLANK

Approved for public release. Distribution is unlimited.

MODELING AND SIMULATION OF THREE-PHASE AC MICROGRID

Charles Y. Hirsch
Commander, United States Navy
BS, U.S. Naval Academy, 2001

Submitted in partial fulfillment of the
requirements for the degree of

MASTER OF SCIENCE IN ELECTRICAL ENGINEERING

from the

NAVAL POSTGRADUATE SCHOOL
March 2020

Approved by: Giovanna Oriti
Advisor

Roberto Cristi
Co-Advisor

Douglas J. Fouts
Chair, Department of Electrical and Computer Engineering

THIS PAGE INTENTIONALLY LEFT BLANK

ABSTRACT

Sustainable power at the forefront of Department of Defense operations is paramount on the battlefield as well as at naval installations around the world, and microgrid technology enables the deployment of renewable energy sources. This thesis develops a physics-based model of a three-phase microgrid set up with three commercial-off-the-shelf (COTS) inverters and a battery bank as its energy storage system. Both the model and the laboratory microgrid can be operated in grid-tied or in islanding mode. The microgrid's voltage waveforms, spectra, total harmonic distortion, and current waveforms are predicted by simulations and measured in the laboratory. IEEE Standard 519 and the manufacturer's performance standards provide the metrics for the power quality analysis. Comparisons of performance of the model to experimental laboratory data determine that the COTS units conform to IEEE Standard 519 and are suitable for further studies into microgrid expansion, management, and employment.

THIS PAGE INTENTIONALLY LEFT BLANK

TABLE OF CONTENTS

LIST OF FIGURES

LIST OF TABLES

THIS PAGE INTENTIONALLY LEFT BLANK

LIST OF ACRONYMS AND ABBREVIATIONS

A	ampere
ac	alternating current
Ah	ampere-hours
COTS	commercial off the shelf
dc	direct current
DER	distributed energy resource
DG	distributed generation
DoD	department of defense
DS	distributed storage
EMS	energy management system
ESS	energy storage system
FFT	fast Fourier transform
FOB	forward operating base
HESS	hybrid energy storage system
kW	kilowatt
Mfg	Manufacturer
NPS	Naval Postgraduate School
PCC	point of common coupling
PWM	pulse width modulation
PI	proportional integrator
SC	super capacitor
SOC	state of charge
SR	set reset
THD	total harmonic distortion
tstep	time step

THIS PAGE INTENTIONALLY LEFT BLANK

ACKNOWLEDGMENTS

I want to thank my thesis advisor Giovanna Oriti and my co-advisors Alex Julian, Roberto Cristi, and Anthony Gannon. Their patience and incredible help allowed me to complete this thesis amid a more than average complicated life. I would also like to give a special thanks to Emily, the mother of my two beautiful boys, Landon and Maddox, for being the cornerstone of our family while I was absent completing this task. Last, but certainly not least, I want to give a special thanks to my fiancée, Kristen, whose daily encouragement kept me to task and helped me reach the finish line with energy to spare.

THIS PAGE INTENTIONALLY LEFT BLANK

I. INTRODUCTION

A microgrid can be described as a controlled collection of distributed energy resources (DER) coupled with energy storage systems (ESS) to deliver power to a range of loads, either while connected to a power grid, or while isolated from the grid [1]. The flexibility and redundancy of a microgrid offers strength to the local power distribution system and ensures vital loads can be powered independently of grid availability.

As an increasing number of commercial-off-the-shelf (COTS) control systems and power converters are being offered to the public, the need still exists to 1) standardize power quality delivered to the end user and 2) ensure that all safety features, both protective system actions and grid protection actions, are synchronized and standardized across the industry. This thesis focuses on the former, specifically studying a COTS implementation of a microgrid and comparing it to its physics-based model.

The Institute of Electrical and Electronic Engineers (IEEE) defines power quality as "The concept of powering and grounding sensitive electronic equipment in a manner that is suitable to the operation of that equipment" [2]. This generalized specification illustrates the necessity to first define the load being powered. *IEEE Standard 1159–2019* provides a list of electrical phenomena that contribute to poor power quality. This listing includes, but is not limited to, the measurement of total harmonic distortion (THD), electromagnetic interference, voltage waveform dips, swells, sag, etc [3]. Furthermore, in the textbook *Power Electronics*, Chapter 11 Table 11–1 provides an example of a power quality envelope for a computer [4]. This envelope is driven by the needs of the load and include factors independent of the load, co-dependent on the interaction between the load and power source, and factors solely influenced by the load.

High frequency harmonics produced by power converters utilizing pulse width modulation (PWM) is a common artifact for COTS converters across the spectrum of manufactures. The inherent process in power conversion induces distortion both in distributed voltage and current. *IEEE Standard 519* [5] specifically provides guidance on

limiting harmonics in power systems, and it is the standard that this study is referenced against.

The Naval Postgraduate School (NPS) microgrid is comprised of three Sunny Island [6] converters which are configured into a three-phase ac system. Each Sunny Island module provides dc to ac conversion from a single dc source. THD measurements at the point of common coupling (PCC) between the converters, the grid, and loads are used to compare and contrast model simulations and adherence to the limits in [5] and [6]. The result will assess the ability of a COTS microgrid to provide acceptable power quality that complies with the recommendations in *IEEE standard 519* [5].

Microgrids are in use across the spectrum of military installations, to include those used on the battle front. The Department of Defense (DoD) funds and maintains these microgrids in order to reduce the carbon footprint, reduce operating costs of facilities, and provide the ultimate flexibility to the warfighter with regard to forward operating base (FOB) placement and operation. As these unique systems evolve, commercial technologies offer alternatives to the expense of system development and maintenance. The question is whether or not these commercial systems can provide the necessary power quality and capacity in the environments of intended use.

A. OBJECTIVE

The focus of this thesis is to develop a physics-based model of the critical portions of an NPS three-phase microgrid to simulate and measure THD at the PCC, as well as provide a working baseline model for future studies of Energy Management System (EMS) control and the addition of alternative DERs. Steady state performance for both the model and the NPS microgrid will be used to measure the THD of each system and conformance to the *IEEE Standard 519* [5], as well as voltage and current generation. This will provide further consideration of the use of COTS components in military applications, including standalone forward operating base (FOB) use.

B. APPROACH

This study evaluates the operation of an installed three-phase microgrid assembled with COTS components. Alterations have been made in order to constrain the system response within the limits of the NPS microgrid and provide repeatable conditions during testing. A physics-based model of this microgrid has been developed and implemented in *MATLAB ® Simulink 2018b* [7]. Using the model, the study analyzes the operation of the H-Bridge inverters both in delivery of power and power quality. Of note, the internal details of the inverters were not available during modeling, therefore, assumptions have been made on the internal operations of the COTS hardware.

Using two scenarios, balanced and unbalanced loading, the three-phase THD is evaluated and compared between the model and the laboratory microgrid. In addition, power loading in both balanced and unbalanced scenarios is evaluated using the load current of the three phases and neutral line. These two attributes are used to confirm model simulated results against the real-world system performance.

This thesis is organized as follows: Chapter II provides the foundation of microgrid configuration and various terms to properly classify a microgrid system. Chapter III describes the three-phase microgrid model which was developed from the laboratory setup. Chapter IV outlines the various standards that the measurements were compared against. Chapter V contains the findings and results of the model to laboratory comparisons. Finally, conclusions and recommendations for future work are presented in Chapter VI.

THIS PAGE INTENTIONALLY LEFT BLANK

II. BACKGROUND

In this chapter, essential terms and concepts related to microgrids are explained. This includes definitions of key terms and descriptions of microgrid operation.

A. SINGLE PHASE MICROGRID

A microgrid is a smaller version of the power grid we are accustomed to today. Power companies provided main line power to each home and business via a transformer from a power line. Microgrids have the critical characteristic of being able to disconnect from the main grid and remain in operation. The power source for a microgrid comes from DERs which [1] are comprised of distributed generation (DG) sources and distributed storage (DS) components. DG sources are solar panels, generators, wind generators, etc. DS components are batteries of many types, super capacitor banks, or other energy storage devices.

Microgrids are operated in two modes, grid-tied and islanding mode. In grid-tied mode, power is fed to the microgrid via the main grid supply and the DERs and DG sources supplement that power provided to the microgrid loads. In islanding mode, the microgrid is disconnected from the main line power and becomes self-sufficient, providing power from both DER and DG components to critical loads.

When a microgrid is developed, it is built to provide a specific amount of power to specific loads. Critical loads are those loads that must remain powered whether in grid-tied or islanding mode while non-critical loads are usually powered only in grid-tied mode and are not essential to operations in islanding mode. Figure 1 illustrates a simplified microgrid.

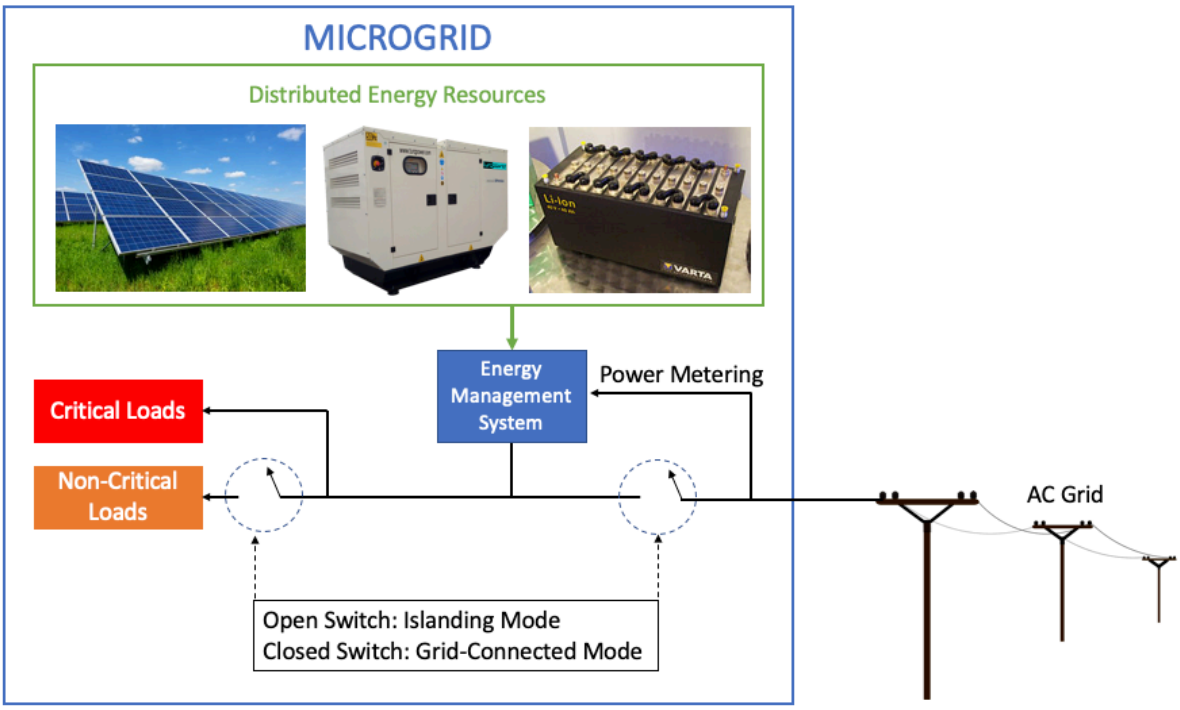

Figure 1. Simplified Microgrid. Adapted from [8].

B. MICROGRID CLASSIFICATION

Topologies of microgrids are categorized by the arrangement and control of the network. In standalone distributed microgrids, sometimes referred to as "nanogrids," the building blocks include DERs, essential and non-essential loads for a single consumer, and a DS called an ESS. Figure 2 illustrates the centralized and standalone microgrids which contain the same components. In a centralized microgrid the ESS resources are combined together to serve a group of consumers. In both cases the microgrids can be connected to the local power grid and this mode is referred to as grid-tied. When the grid is not providing power to the microgrid, the microgrid is said to be in islanding mode.

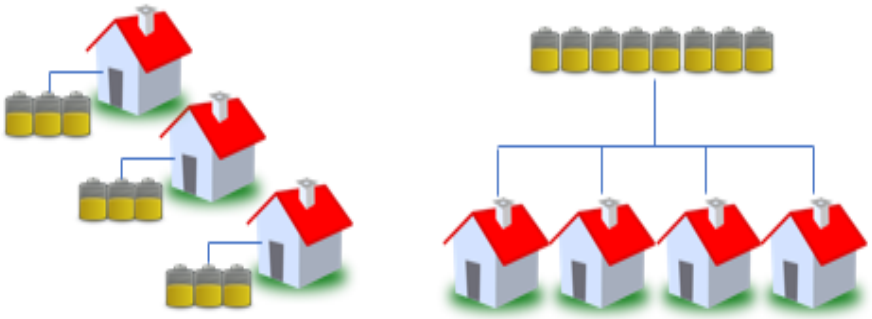

Figure 2. Standalone Microgrids vs. Centralized Microgrid. Adapted from [7].

The ESS is further categorized by its composition. ESSs that are comprised of more than one type of device are referred to as a hybrid ESS (HESS). An ESS is an energy storage device of a single type.

Another classification method concerns the configuration of the ESS/HESS and required control mechanisms. The ESS/HESS may or may not require a control interface in order to meet parameter specifications when supplying power to the load. For example, a super capacitor (SC) may have maximum open circuit voltage of $65V_{dc}$. In order to interface with the parameter-controlled direct current (dc) bus of $40V_{dc}$, the capacitor voltage must be regulated down to $40V_{dc}$. This type of system is referred to as a semi-active ESS [10]. A configuration that requires no control mechanism is simply referred to as a passive ESS.

The focus of this study is the evaluation of an active ESS. An active ESS is a system in which power flow is both from and to the ESS. This provides the ability to discharge power from the ESS, and when in grid-tied mode, charge the ESS. Placing dc/dc converters between each component of the ESS and the bus of interest makes this possible.

The final classification attribute concerns the varying microgrid architectures. Four architectures exist: centralized dc bus, centralized alternating current (ac) bus, distributed ac bus, and hybrid coupled bus [11]. In a centralized dc bus architecture shown in Figure 3, the HESS (including ac sources) uses ac/dc and dc/dc converters to provide power to a

common dc bus. This is then converted by a dc/ac converter to a subsequent ac bus. Of note, power flow is in one direction.

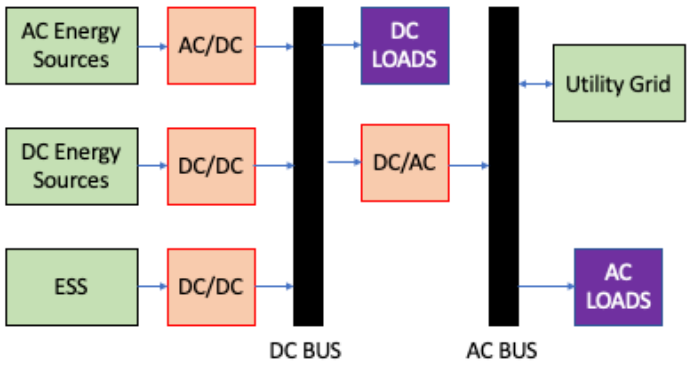

Figure 3. Centralized dc Bus Architecture. Adapted from [11].

In a centralized ac bus architecture [11], all energy sources are converted to ac to supply a common ac bus seen in Figure 4.

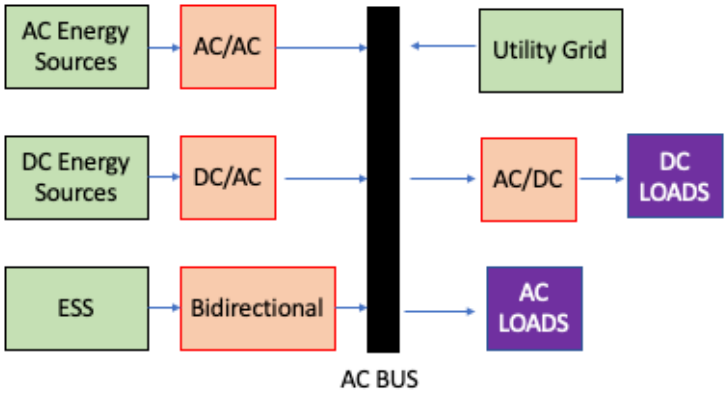

Figure 4. Centralized ac Bus Architecture. Adapted from [11].

The third architecture depicted in Figure 5 is the distributed ac bus. This architecture centralizes the grid power and provides ac converters to each element in the microgrid.

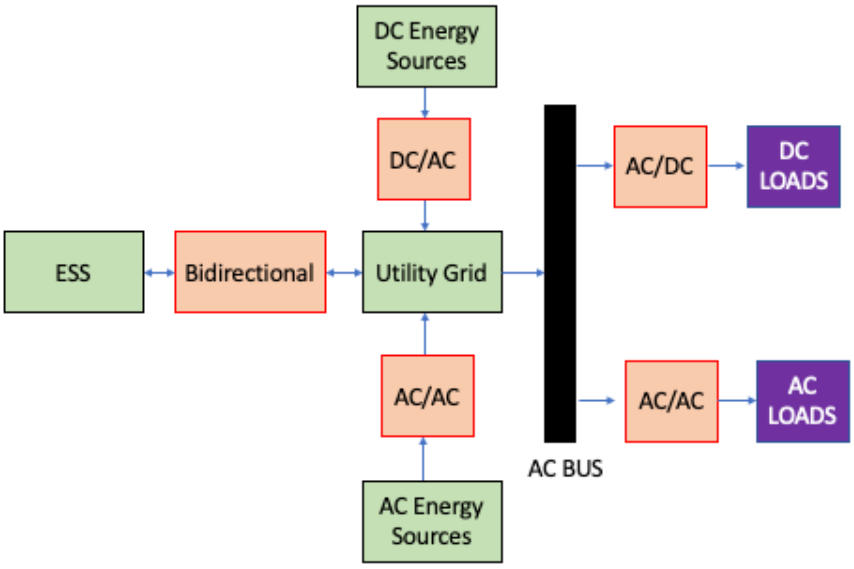

Figure 5. Distributed ac Bus Architecture. Adapted from [11].

The final architecture, and the one that will be the focus of this paper, is the hybrid coupled ac/dc bus. In this system there is a dc and ac bus. Conversion between both busses is accomplished by a bi-directional converter. This distinguishes a hybrid coupled bus from a centralized dc bus where power flow is in one direction [11]. Figure 6 illustrates this architecture.

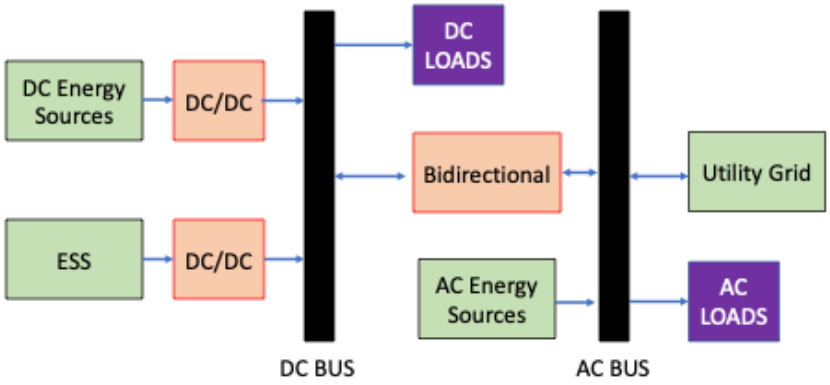

Figure 6. Hybrid Coupled Bus Architecture. Adapted from [11].

This paper will discuss the performance of the modeled standalone active distributed hybrid coupled microgrid in islanding mode. This performance is directly compared to the actual realization of the COTS microgrid. In addition to power quality performance, the physics-based model and actual microgrid are compared to military and the manufacturer specifications.

C. THREE-PHASE POWER

In this thesis we will be referring to a specific three-phase power microgrid located at the Naval Postgraduate School in Monterey, California. This system is constructed with SMA Solar Technology COTS components and provides the operating limits for this model [6]. In order to generate a three-phase signal from the microgrid characterized in Figure 7, three H-Bridge converters were placed in parallel, each one providing a single-phase ac waveform. The master unit provides signaling to the two slave units with information to create the necessary phase shifted waveforms. Figure 7 illustrates the configuration of three Sunny Islands 6048-US-10 in parallel to generate three-phase ac [6].

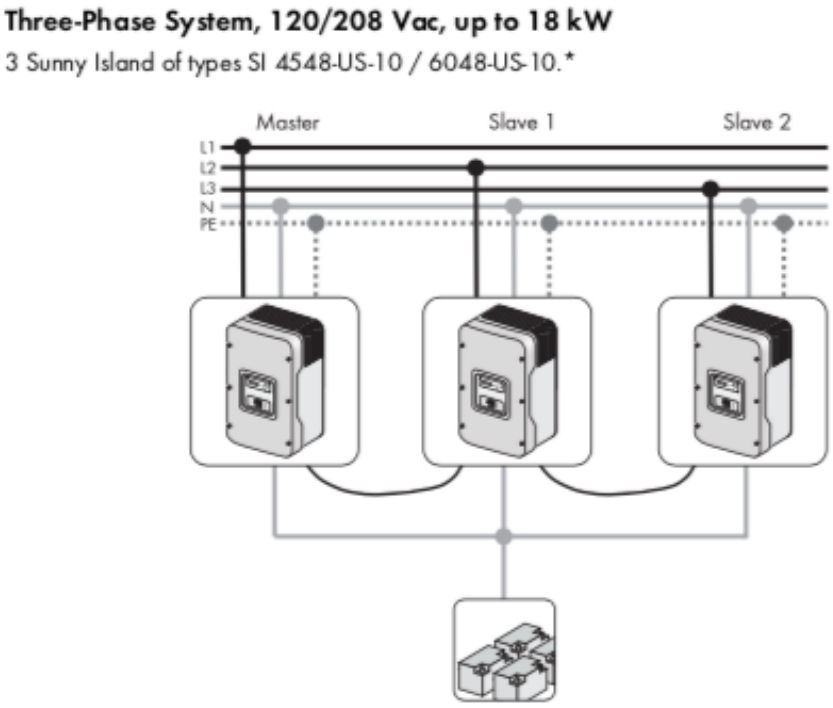

Figure 7. Sunny Island Three-Phase Inverter Configuration. Source:[6].

D. NPS MICROGRID AND LABORATORY SETUP

The NPS microgrid is comprised of three COTS converters manufactured by SMA, Inc. These three converters are configured as in Figure 7. Figure 8 [12] depicts the microgrid in the laboratory. The model described in Chapter III omits all DERs associated with this microgrid with the exception of the $48V_{dc}$ battery bank. Figure 8 shows the laboratory setup for data collection. A three-phase breaker panel acts as the PCC or primary distribution node for the three converters. Power is supplied to the panel via a supply breaker and the critical and non-critical loads are powered from the panel. In this thesis, the three-phase 14.5Ω/29Ω WYE connected resistor bank is used as the only three-phase load. Figures 9 and 10 provide a system overview and diagram. Figures 11 through 13 depict components of the data collection setup. Appendix A details the setup of the data collection instrumentation.

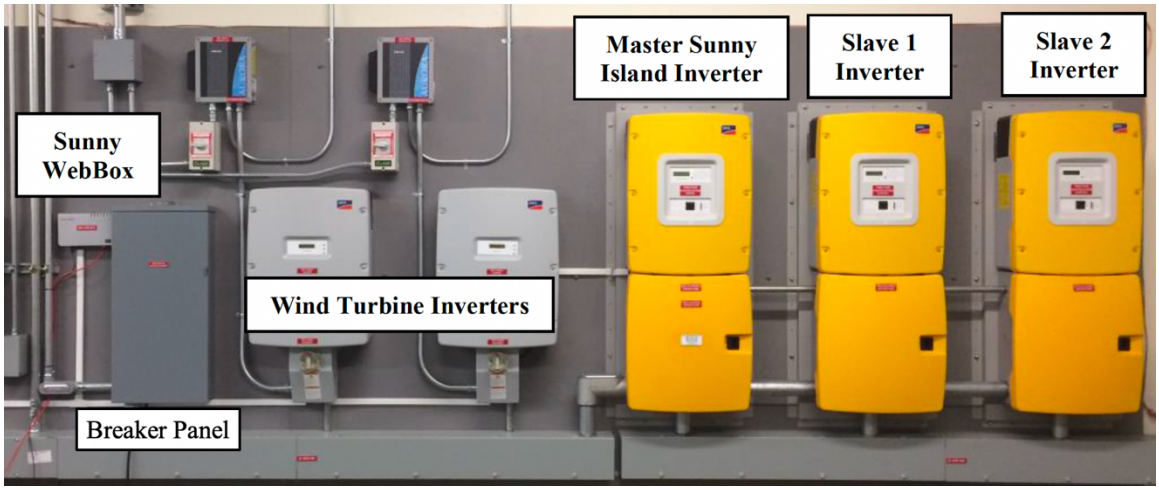

Figure 8. NPS Microgrid Laboratory. Source: [12].

Figure 9. Microgrid Laboratory Breaker Panel Data Collection Setup

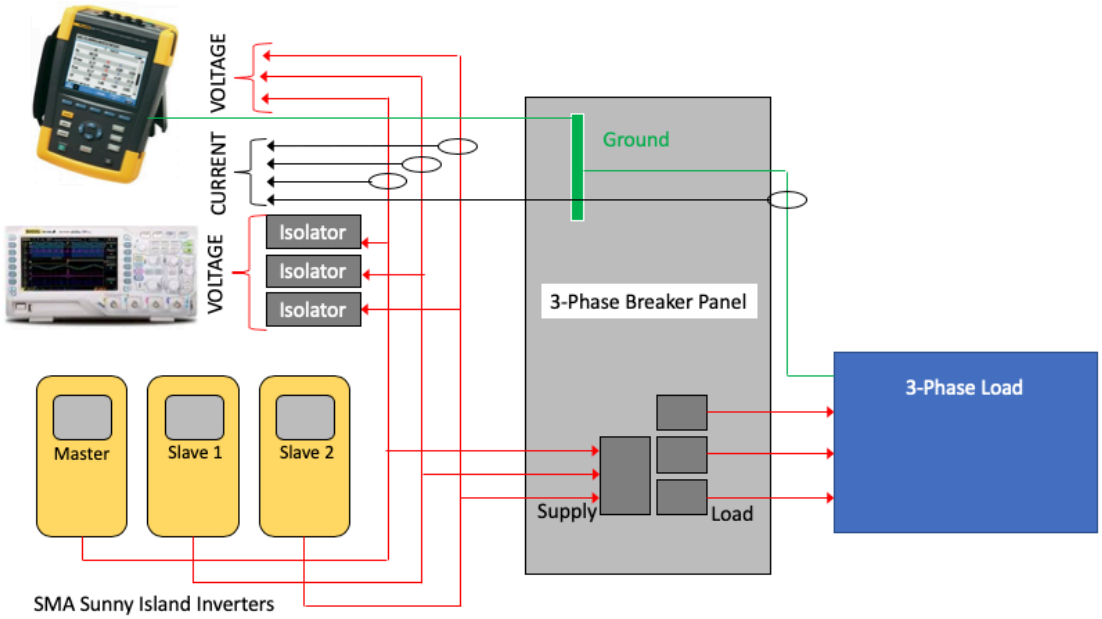

Figure 10. Microgrid Data Collection Diagram

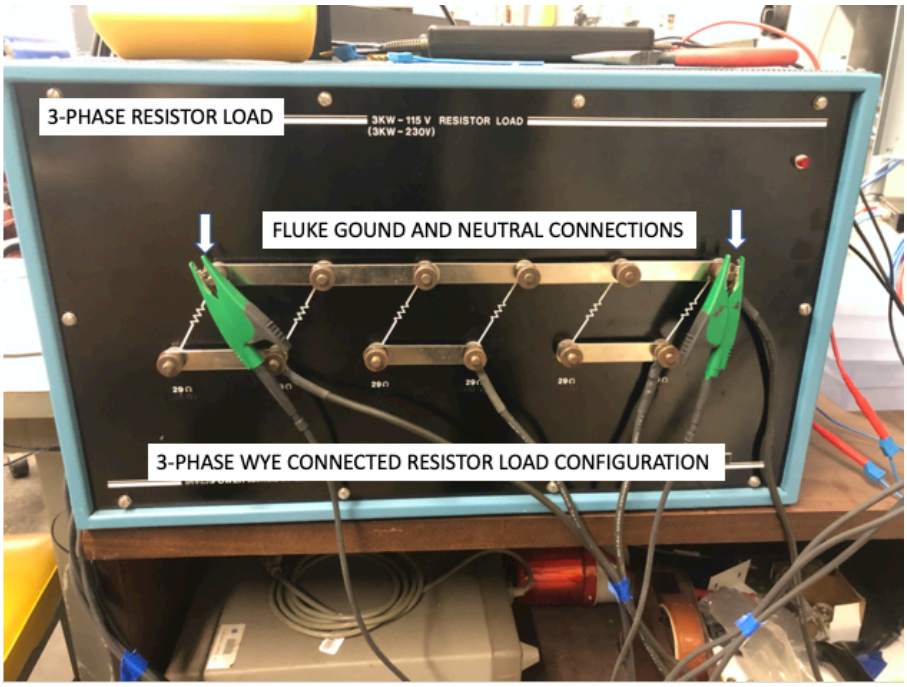

Figure 11. Three-phase Resistor Load and Fluke Grounding

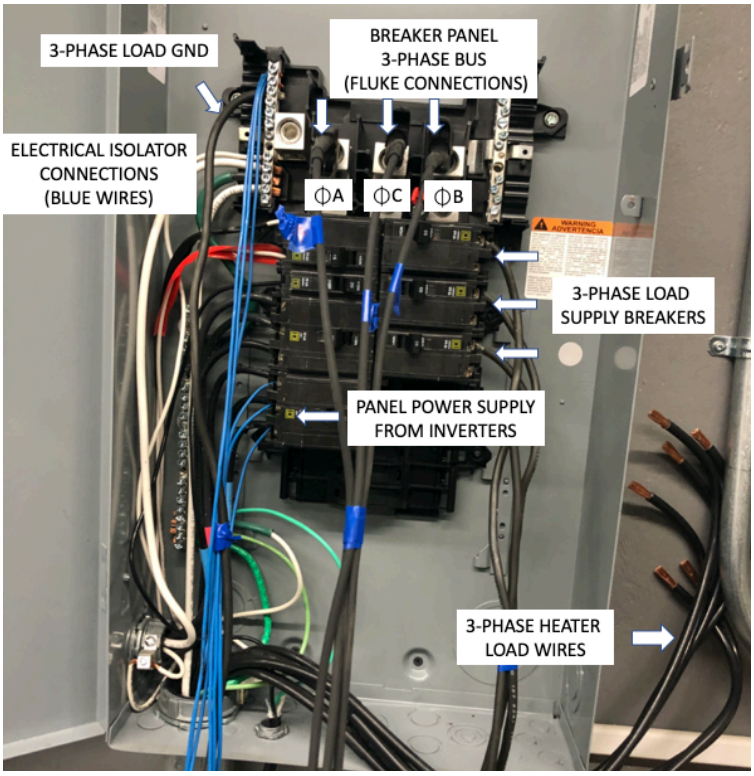

Figure 12. Microgrid Distribution Panel

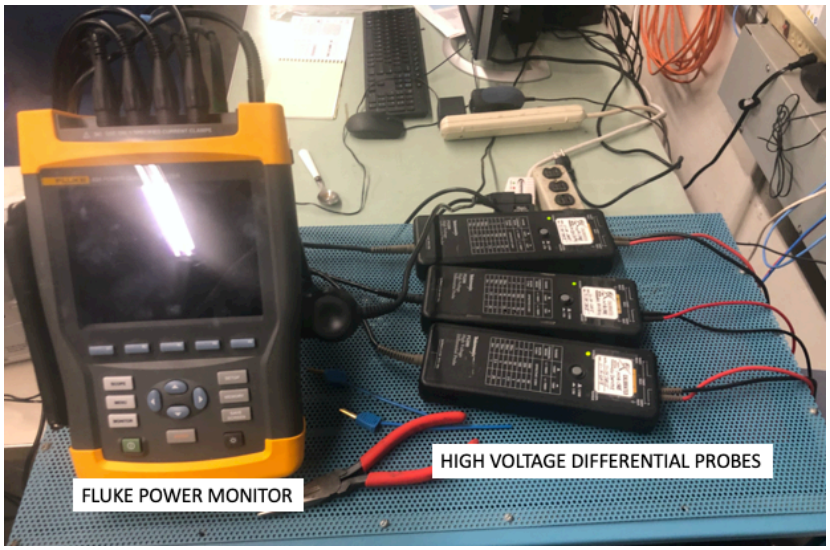

Figure 13. Data Collection Peripherals

Figure 14 outlines the construction of the NPS microgrid to include all DG sources, associated inverters and converters, and loads. Photovoltaic cells and the vertical axis wind turbines will not be used as DG sources. This thesis will focus solely on the use of a resistive bank mimicking the heater load and will neglect the operation of the refrigeration plant.

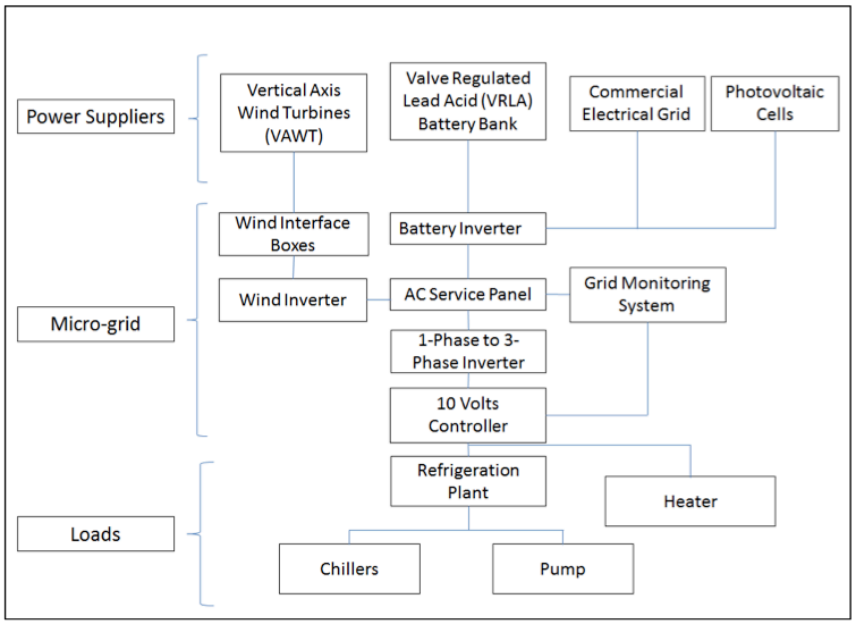

Figure 14. NPS Microgrid Configuration. Source: [12].

Figure 15 and Figure 16 illustrate the architecture of the microgrid under study. Figure 16 represents a simplified model of a hybrid coupled bus which mimics the NPS microgrid. It also is the blueprint for the physics-based model which is discussed in detail in Chapter 0. An image of the SIMULINK implementation of the physics-based model is provided in Appendix B.

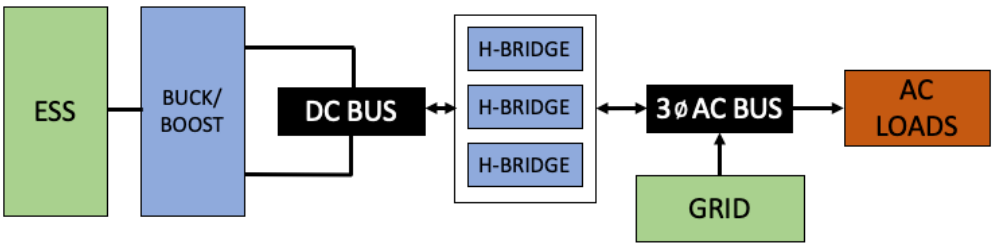

Figure 15. Simplified Hybrid Coupled Bus Microgrid

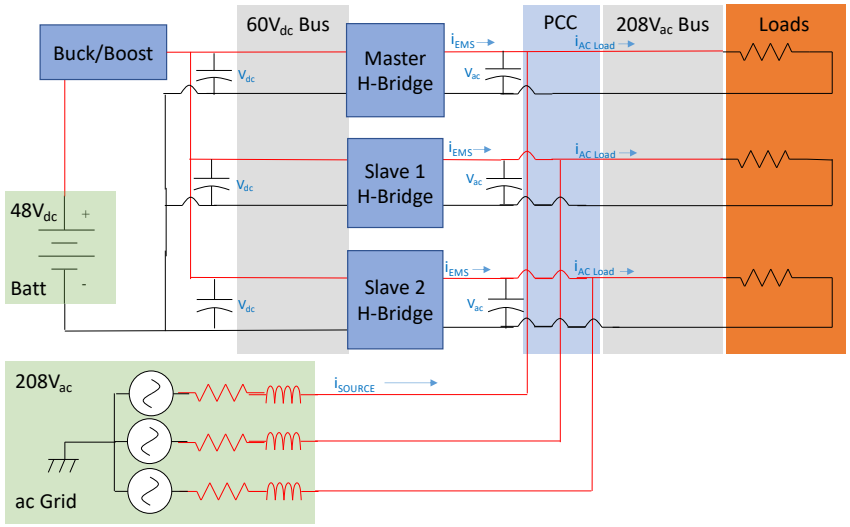

Figure 16. Circuit Schematic of the NPS Microgrid Used to Create the Physics-Based Model

THIS PAGE INTENTIONALLY LEFT BLANK

III. NPS MICROGRID MODEL

This chapter details each component of the microgrid model and how they interface to deliver power to the load.

A. ENERGY MANAGEMENT SYSTEM

At the heart of a microgrid is the control unit that senses, adjusts and delivers required power to the loads within the microgrid. Using specific control parameters, the power electronics-based Energy Management System (EMS) [13] is responsible for providing regulated voltage and current to the microgrid, whether in grid-tied or islanding mode. In the physics-based model developed for this thesis, the buck/boost and H-bridge converters are the power electronics elements in the EMS. These structures will be explained in detail in the following section.

B. MODEL COMPONENTS

The major components of the microgrid model are described in this section. This physics-based model was developed to simulate the behavior of the microgrid system assembled in one of the NPS laboratories using COTS materials. *MATLAB*® and *SIMULINK R2018b* [7] have been used to implement the physics-based model. Assumptions based on state-of-the-art power electronics were made when the internal parameters of the COTS converters were not available from the manufacturer.

1. Battery

The physics-based model developed for this study includes a simplified battery model. Observations of performance are at steady state and at small time intervals. Therefore, the effects of temperature, age, and state of charge (SOC) are neglected in the battery voltage output. The battery model uses an internal resistance (R_O) and has a total capacity of 200 amp-hours (Ah). The SOC is approximated by book-keeping estimation using the Coulomb counting method shown in the following equation.

$$SOC(t) = SOC(t-1) \bullet \frac{I(t)}{Q_n} \bullet \Delta t$$

The current capacity is represented by the previous SOC multiplied by the output current *I(t)*. Nominal capacity of the battery is represented by Q_n. Figure 17 provides the *SIMULINK* [7] implementation of the battery.

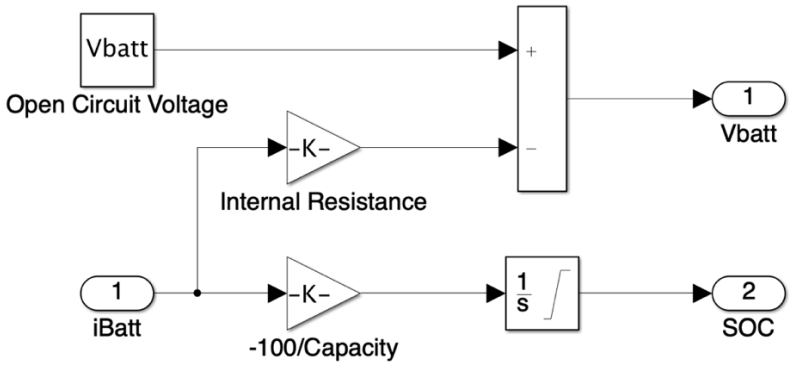

Figure 17. Battery Model

This model has limitations in scenarios that require longer time or ones that need scalability of realistic multi-parameter battery response; however, it is valid for the analysis presented in this thesis. All battery management functions are controlled by the COTS converter and are neglected in this model because they are not available from the manufacturer and are not relevant to the power quality analysis presented here. Table 1 contains the specifications of the battery model.

Table 1. Battery Specification

Capacity	200Ah
Internal Resistance	5mΩ
Open Circuit Voltage	$48V_{dc}$
Continuous Charging Current	110A

2. Power Grid

The power grid provides three-phase power to the microgrid when in grid-tied mode. Figure 18 provides the circuit schematic of the wye connected three-phase voltage source from the main grid, including estimated line inductance and resistance.

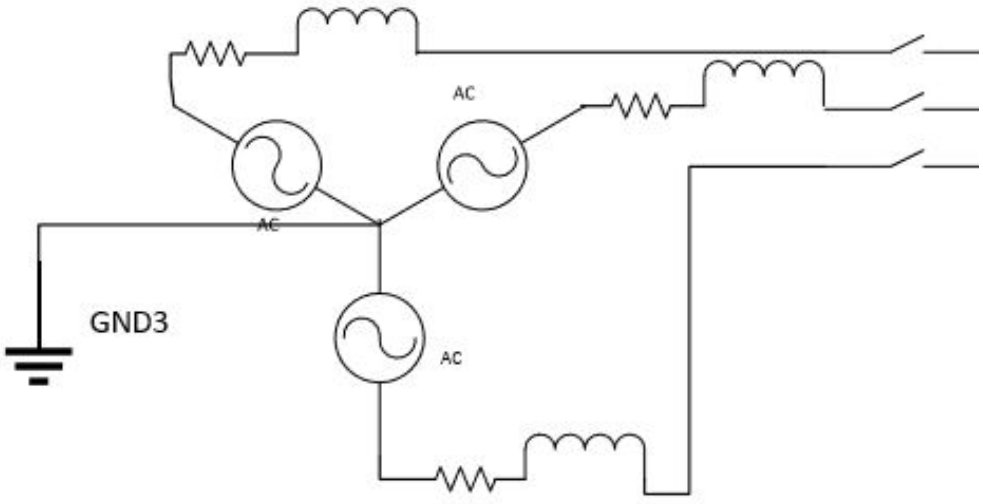

Figure 18. Three-Phase Voltage Source to Model the Main ac Grid

Figure 19 is the *SIMULINK* [7] implementation of the three-phase voltage source shown in Figure 18. In addition to the three-phase currents, a fourth output labeled "Grid On Off" is the signal line to the three H-Bridge inverters to simulate closing or opening of the grid disconnect switch.

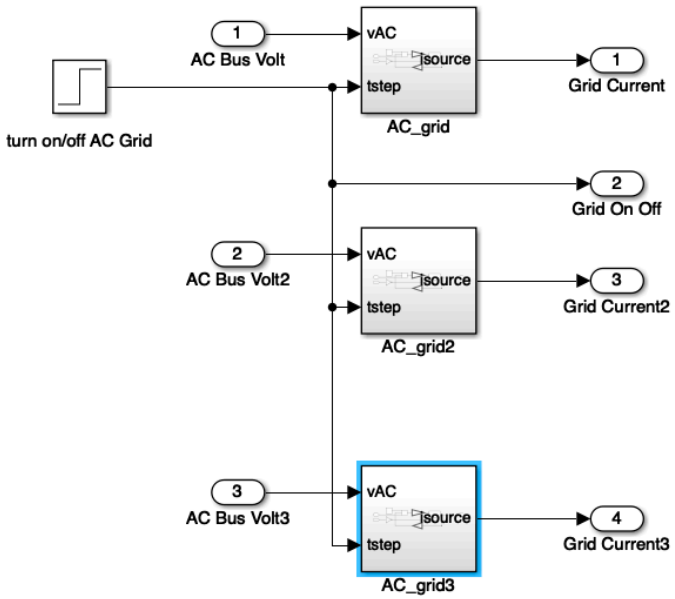

Figure 19. Three-Phase Grid Model

Figure 20 is an implementation of a single phase of the three-phase grid in *SIMULINK* [7]. The timestep (tstep) input signals the actuation of the grid disconnect which in turn triggers the integrator block to output grid source current. Harmonics are injected into the pure sine waveform in order to replicate laboratory measurements. Figure 21 illustrates the harmonic injection into the base sine wave. Table 2 lists the values of the main grid parameters used for the simulations.

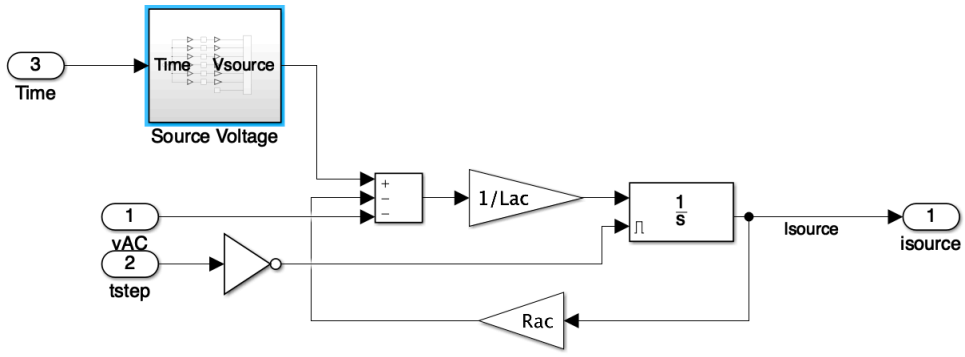

Figure 20. Single Phase of Grid Source Model

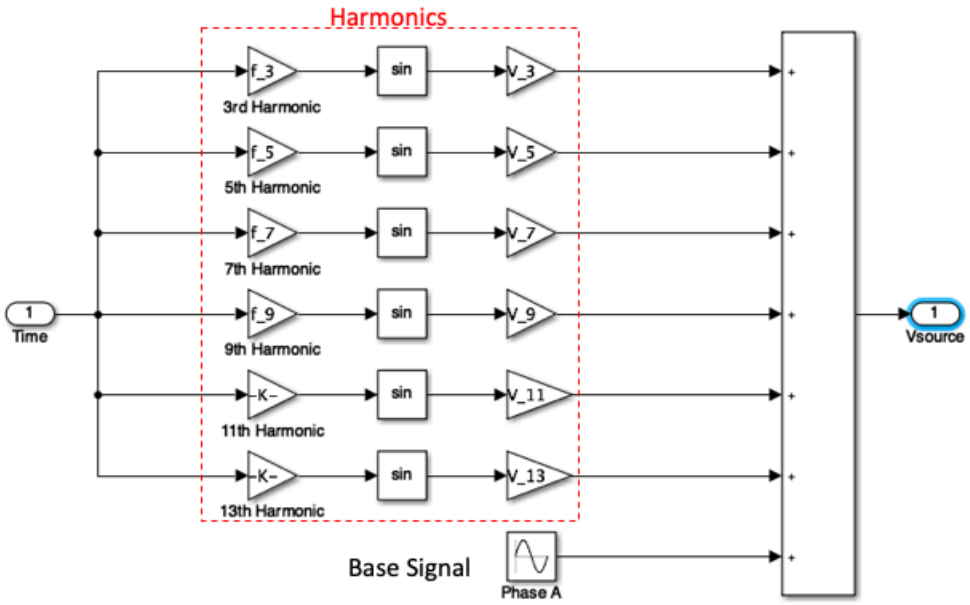

Figure 21. Grid Source Harmonic Injection. Source: [8].

Table 2. Grid Specification

Voltage	$108V_{AC}$
Frequency	60Hz
Inductance	6μH
Resistance	1mΩ
Harmonics	3rd, 5th, 7th, 9th, 11th, 13th

3. Buck Boost Converter

The buck/boost converter regulates the dc bus voltage at $60V_{dc}$ +/- $5V_{dc}$. It is comprised of a Proportional Integrator (PI) controller which activates either the buck or boost to operate. A boost converter will increase the input voltage, while a buck converter will reduce the input voltage. These two work together to provide a regulated, constant dc bus voltage. The boost converter operates to provide power to the dc bus while the buck converter operates when power flows from the dc bus to the batteries, which occurs during charging operations. Figure 22 illustrates the buck/boost converter as it is implemented in *SIMULINK* [7].

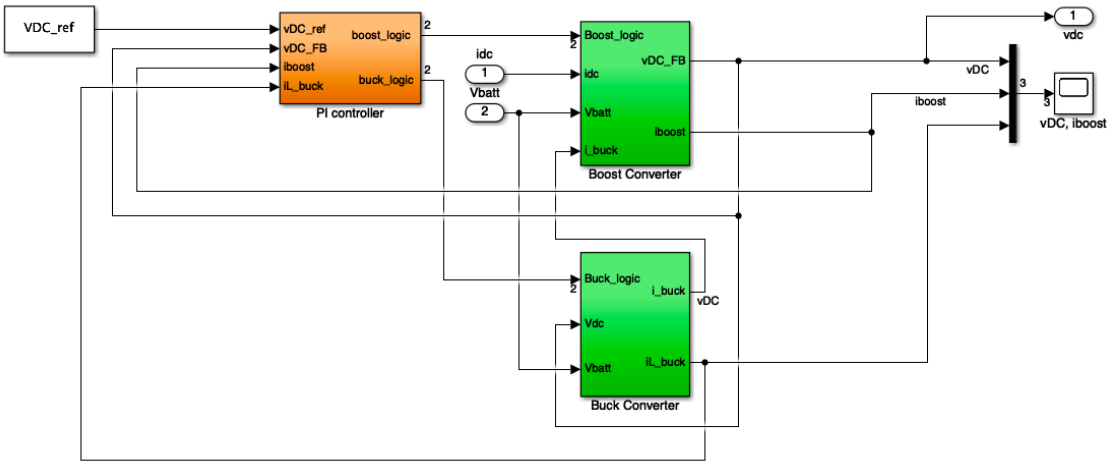

Figure 22. Buck/Boost and PI Control Model

4. Control

The PI controller executes logic using a hysteresis band to enable the buck or boost circuitry. Using the dc bus feedback voltage, the controller compares the voltage to the upper and lower limits of the hysteresis band. The band used for this model is +/- $3V_{dc}$. If the dc bus feedback voltage is less than $V_{dc\_reference}$ - $3V_{dc}$, a Set Reset (SR) flip flop sends a signal to enable boost and disable buck. The opposite is true when feedback voltage is greater $V_{dc\_reference}$ + $3V_{dc}$. Figure 23 block diagram illustrates the flow of the buck/boost controller. The specification for this control is located in Table 3.

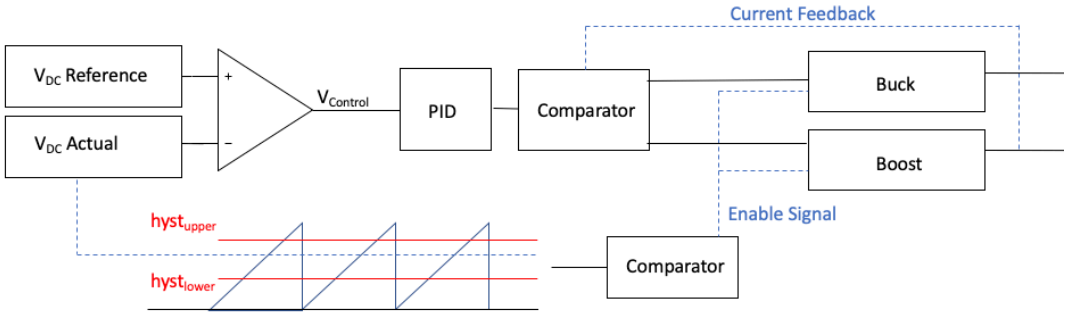

Figure 23. Simplified Buck/Boost Control Diagram. Adapted from [4].

Table 3. Proportional Integrator Controller Specification

Switching Frequency	3kHz
Upper Hysteresis Band	$63V_{dc}$
Lower Hysteresis Band	$57V_{dc}$

5. Buck Converter

The buck converter is responsible for reducing the dc bus voltage to maintain it within the acceptable ranges to reference voltage. Specifically, buck is enabled when $V_{dc\ Bus}$ is greater than the hysteresis upper limit, therefore power from the ac grid is used to charge the batteries. Figure 24 illustrates the buck converter circuit and Table 4 provides its specification. The position of the switch allows charge accumulation in the inductor when closed and discharge when opened. The output voltage is controlled by changing the duty ratio (D) of the switch. In an ideal system, in continuous conduction mode, the average output voltage can be calculated using the following equations.

$$D = \frac{t_{ON}}{T_S} = \frac{v_{control}}{\hat{V}_{st}}$$

$$V_O = \frac{1}{T_S}\int_0^{T_S} vO(t)\,dt = \frac{1}{T_S}\int_0^{t_{ON}} V_d\,dt + \int_{t_{ON}}^{T_S} 0\,dt = \frac{t_{ON}}{T_S}V_d = DV_d$$

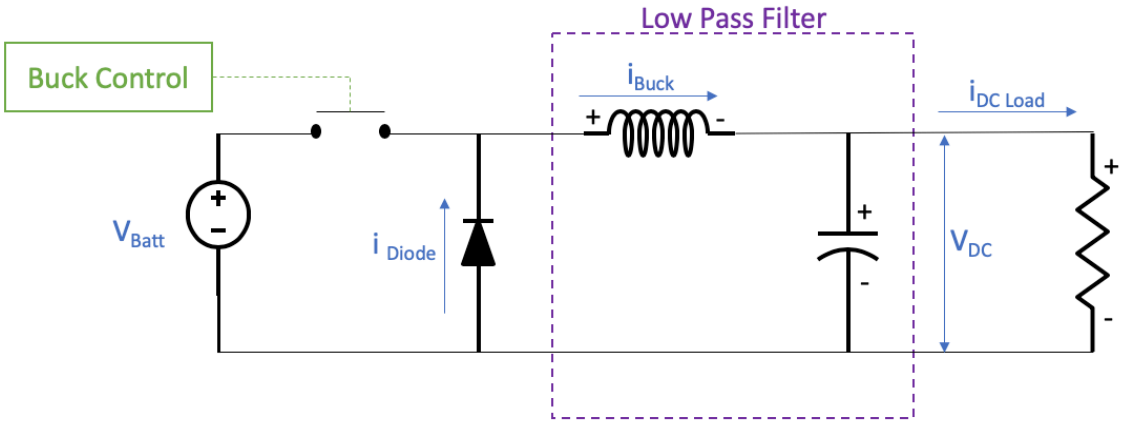

Figure 24. Buck Converter. Adapted from [4].

Table 4. Buck Circuitry Specification

Inductor (L)	1.50mH
Inductor Resistance (R_L)	0.05Ω
Capacitor (C)	300μF

6. Boost Converter

The boost converter is responsible for increasing the dc bus voltage to maintain it within the acceptable range to reference voltage. Specifically, boost is enabled when $V_{dc\ Bus}$ is less than the hysteresis lower limit and when the batteries send energy to the microgrid. When the microgrid is in grid-connected mode, ac bus voltage is regulated by the grid and power flows from the ac to dc sides of the converter, charging the batteries and raising the dc voltage of the batteries. When in islanding mode, power flows from the batteries to the ac loads, utilizing the boost circuitry to maintain dc bus voltage as battery voltage drops from discharge. Figure 25 illustrates the boost converter circuit.

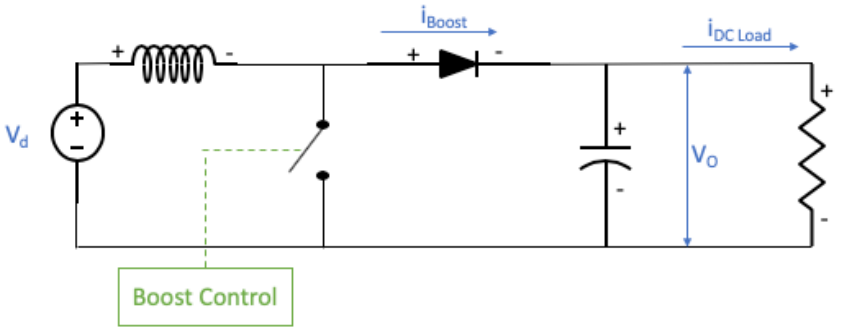

Figure 25. Boost Converter. Adapted from [9].

The specifications for the boost converter are provided in Table 5. The average output voltage in continuous conduction mode can be calculated by the following equations:

$$V_d t_{ON} + (V_d - V_o) t_{OFF} = 0$$

$$V_o = \frac{T_s}{t_{OFF}} V_d = \frac{1}{1-D} V_d$$

Table 5. Boost Circuitry Specification

Inductor (L)	200μH
Inductor Resistance (R_L)	0.05Ω
Capacitor (C)	300μH

7. H-Bridge Converter

The purpose of the H-Bridge inverter is to take dc voltage input and convert it to a single-phase ac output. When in grid-tied mode of operation, the H-Bridge takes the incoming ac current and converts it to dc current in order to charge the batteries. In this model, the three inverters were modeled after the SMA Sunny Island 6048-US off-grid converter [6]. The converter sits between the ac and dc busses providing power in both directions as determined by the state of the grid disconnect. Each converter uses pulse width modulation (PWM) in order to cycle switch sets to generate a single phase of the ac sinewave output. Figure 26 illustrates the incoming triangular waveform and ac waveform input into a comparator. The comparator generates a binary signal where each pulse width is equivalent to the time intersection of the original ac waveform and the triangular wave. This becomes the signal for a single set of switches and results in half of the waveform depicted in the final image of the figure. The negative half cycle of the source ac waveform generates the resulting negative portion of the output ac waveform.

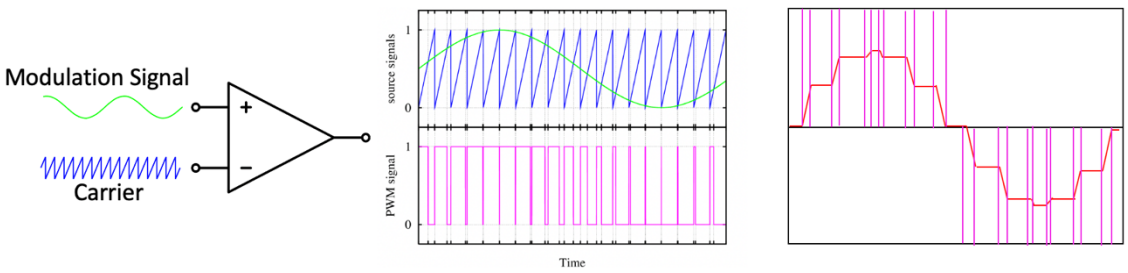

Figure 26. Generation of PWM Signal and Resulting Switched ac Wave Form. Adapted from [4], [14].

Figure 27 illustrates the positive half cycle from the PWM signal to a single-phase ac output. In addition, it demonstrates the circuit current flow path created when the paired switches are closed. In the opposite cycle, the current flow is reversed through the load and generates the negative second half cycle of the ac output.

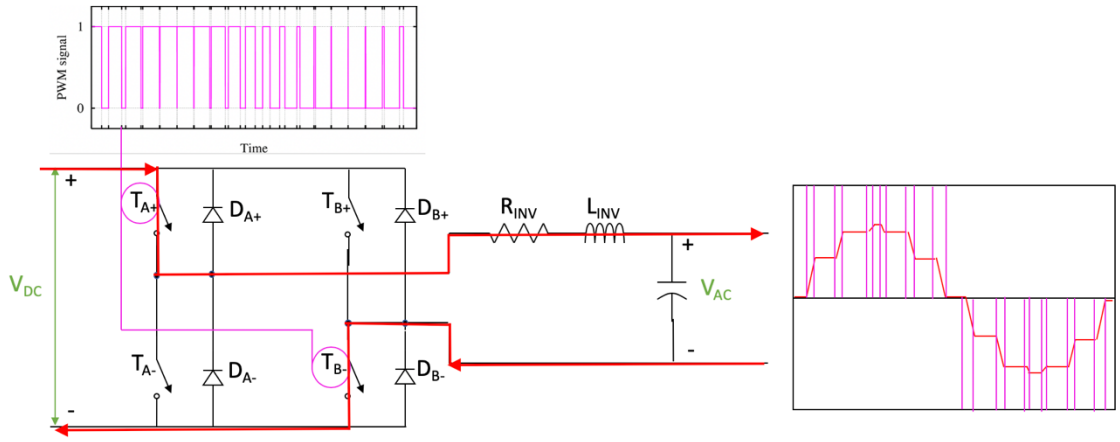

Figure 27. Circuit Diagram of H-bridge Switching and Waveform Formation. Adapted from [4], [14].

The three inverters are configured in a slave/master control scheme. The master inverter provides information to the slave inverters in order to generate the necessary phase shifts for each of the other two phases. Each inverter is responsible for a single phase of the total three-phase system. Figure 28 illustrates the master H-Bridge implementation in *SIMULINK*.

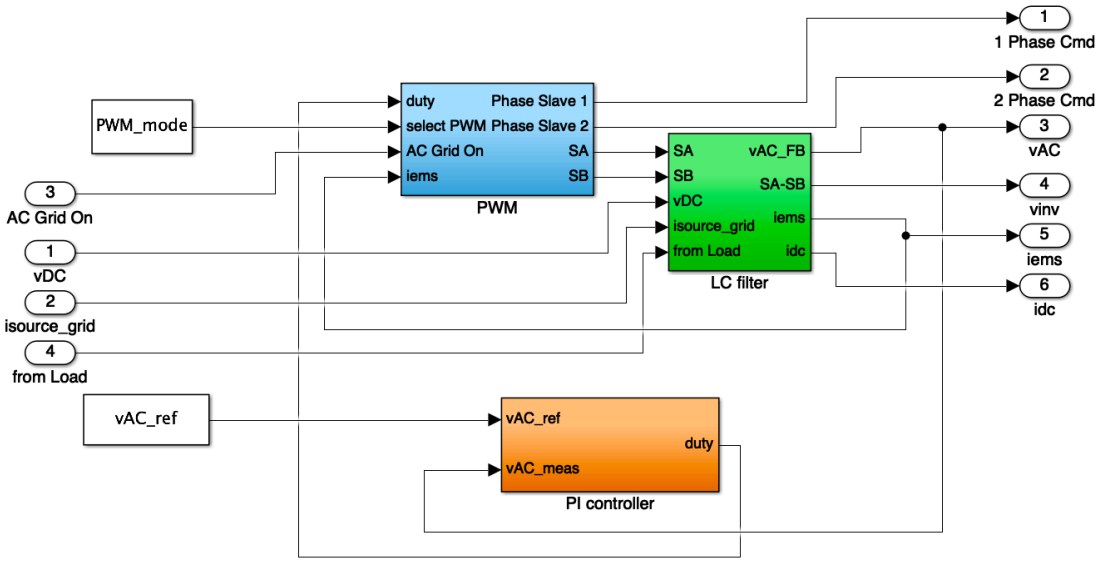

Figure 28. H-Bridge Inverter Model

Each inverter has a 60Hz transformer isolating the H-bridge and providing galvanic isolation according to safety specifications. The transformer also boosts the output voltage of the inverter to the required ac bus voltage. This model uses an ideal implementation of the 60Hz transformer. Table 6 provides the specification of the H-bridge inverter model.

Table 6. H-Bridge Specification

V_{ac} Nominal	$120V_{ac}$
Frequency Nominal	60Hz
Power Nominal (1ϕ)	5,750W
Power Max (3ϕ)	18kW
ac Current Nominal	48A
Switching Frequency	3kHz
Capacitance	3μF
Inductance	0.8mH
Max ac Input Current	56A
Max ac Input Power	6.7kW
Max / Min Input Voltage	$41V_{dc}/63V_{dc}$
Transformer Turns Ratio	1:2

In this research, the laboratory microgrid uses three phases of power to operate a balanced three-phase resistive load. This is also modeled and configured as a wye-connected resistive load. Figure 29 is the circuit schematic of the three-phase heater load.

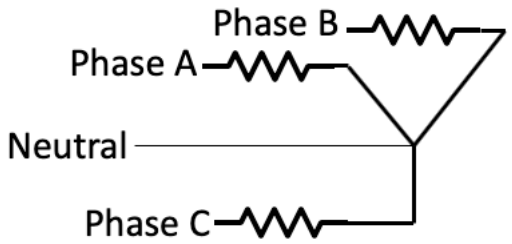

Figure 29. Physical Three-Phase Heater Load Circuit

Figure 30 illustrates the *SIMULINK* [7] implementation of the ac load scenarios. Each leg of the load represents one of two scenarios further explained in Chapter IV. The balanced scenario load is comprised of 3 wye-connected resistors of 14.5Ω. The unbalanced scenario has 2 phases of 14.5Ω loads and a single phase with a 29Ω load.

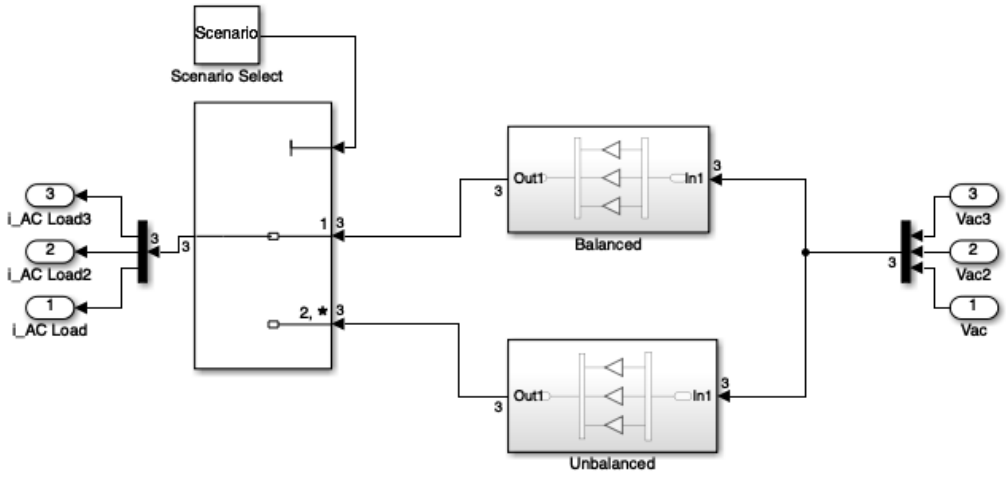

Figure 30. Load Scenario Model

As stated, this research studies a hybrid coupled ac/dc bus. Figure 6 illustrates a simplified view of the system under study where a single $60V_{dc}$ bus is maintained by the Buck/Boost circuitry and transfers current to the 3 H-Bridge converters. Each converter generates a single phase of the three-phase $120V_{ac}$ bus.

THIS PAGE INTENTIONALLY LEFT BLANK

IV. PERFORMANCE COMPARISON

A. SYSTEM SPECIFICATIONS

In addition to the specifications provided for each component, the following system operating constraints are applied to the microgrid:

- dc bus must remain between $41V_{dc}$ and $63V_{dc}$ in order to provide the correct voltage band for the inverters.
- Battery charging current cannot exceed 110A.
- Microgrid loading cannot exceed 100% of power capacity while in grid-tied mode.

B. REFERENCE SPECIFICATIONS

The *IEEE 1100* [2] definition of power quality is used for the purposes of this paper as well as the manufacturer specifications [6]. At the time of writing this paper, the author could not identify power quality standards specific to microgrids. The power quality attribute of THD from *IEEE 519* [5] is used in this study.

The following specifications are used as comparative standards with regard to THD.

THD as stated in *IEEE 519* [5] is 8% in the voltage waveform.

THD specification stated by the manufacturer for each Sunny Island unit is 3% in the voltage waveform [6].

C. SIMULATED SCENARIOS

The following scenarios have been chosen to assess the ability of the microgrid to conform to the THD specifications listed in section B during both balanced and unbalanced load operations:

(1) Balanced load: Three-phase system with a three-phase purely resistive load of 14.5Ω resulting in a power draw of 1.59kW. Model operating in steady

state. This data will prove conformance to the selected standards and demonstrate model adherence to actual system performance.

(2) Unbalanced load: Model operating with unbalanced three-phase load. Specifically, phase B has a resistive load of 29Ω while phases A and B have resistive loads of 14.5Ω. This analysis demonstrates the stability of the system when a load mismatch occurs on a single phase.

D. MEASURE OF COMPARISON

1. Total Harmonic Distortion

THD is "the ratio of the root mean square of the harmonic content, considering harmonic components up to the 50th order and specifically excluding inter-harmonics, expressed as a percent of the fundamental" [5]. This distortion is caused by non-linear loads such as power electronic equipment, transformers, rotating machinery, as well as switching devices present in power converters. THD is one of several indices used to quantify power quality [1] in an electric power system. By evaluating the harmonics using the Fourier series, individual harmonics can be identified as depicted in an example in Figure 31.

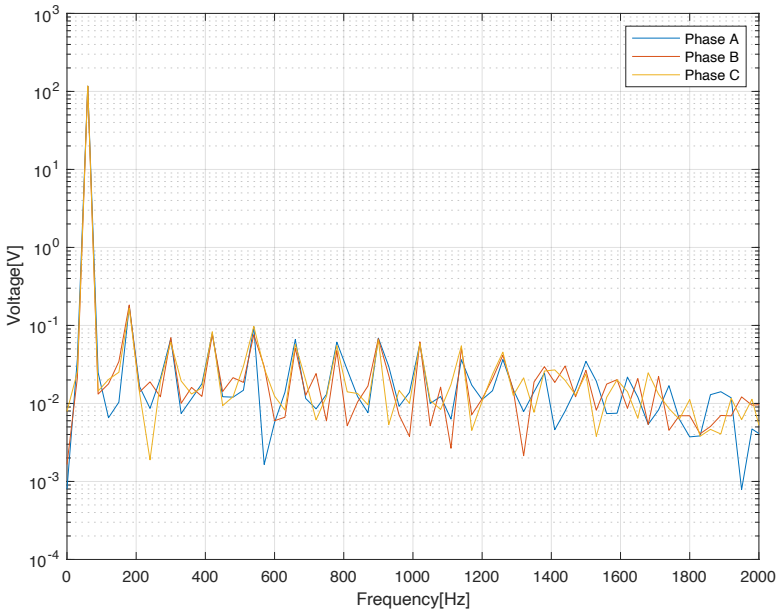

Figure 31. Example Harmonic Response of a Three-Phase System

In order to illustrate the effect of THD on power quality, the power factor (PF) must be defined as the ratio between active power and apparent power [4]. In an entirely resistive circuit, the active power equals the apparent power and PF=1, meaning 100% of the average power is being delivered to the load. Inductive or capacitive circuits reduce PF below 1 due to the reactive power nature of these components as illustrated in Figure 32. PF is mathematically defined as [4]

$$PF = \cos(\theta_v - \theta_i),$$

where θ_v is the phase of the voltage and θ_i is the phase of the current.

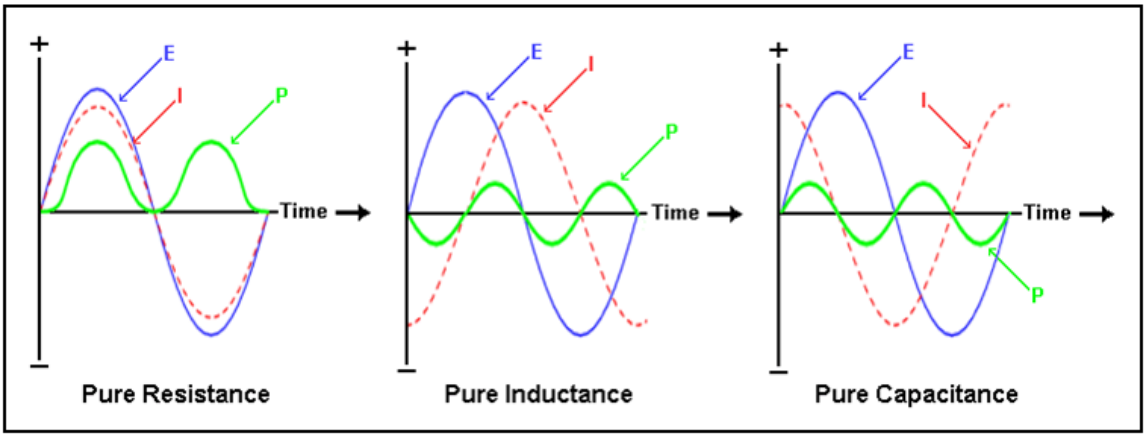

Figure 32. Power Factor Shifting Due to Reactive and Real Loads
Source: [15].

THD is calculated using the following equation [4]

$$THD_V(percent) = 100 \cdot \sqrt{\sum_{h \geq 2} \left(\frac{V_h}{V_{fundamental}} \right)^2}$$

where:

V_h is the rms voltage of the individual harmonics

$V_{fundamental}$ is the fundamental frequency rms voltage

Furthermore, the PF calculation can be broken down into the following [4]

$$PF = \cos(\theta_v - \theta_i) \cdot \sqrt{\frac{1}{1 + THD^2}}$$

Here you can see the significance of THD on PF and thus its impact on power quality. The THD standard of *IEEE 519* [5] will be evaluated in islanding mode for voltage.

2. Load Current

In addition to THD, the time-domain waveforms of the load current are simulated and compared to the experimental waveforms measured in the laboratory microgrid. This comparison validates the model performance under the two load scenarios. Accurate estimation of load current by power provided by the converters is fundamental to the proper simulation of their performance.

3. Voltage Waveform

Output voltage comparisons are made as well as any observations of waveform deformation in each loading scenario. The THD is derived from the ac waveform using the Fourier analysis, but a separate objective comparison is made to demonstrate accurate simulation output. Characteristics from *IEEE 1159* [3] are subjectively applied to the resultant inverter output waveforms.

V. RESULTS

A. METHOD

The results obtained from both the physics-based model simulations and the laboratory measurements are presented in this chapter. The layout of the following section will compare each attribute as follows, THD, output ac voltages, and load currents, between the model and laboratory in each scenario. The findings of the results will be addressed in the conclusion.

B. OUTPUT VOLTAGE HARMONICS AND THD

The THD is computed summing the first 50 harmonics, covering the first 1500Hz of harmonic response and is congruent with the guidelines in [5]. The specific switching frequency of the COTS inverters in the laboratory is unknown, but estimated by inspection of the output waveforms in the time and frequency domain. Therefore, the switching frequency of the inverters in the physics-based model is set at 3kHz. The selection of the frequency range for the THD analysis will preclude the disturbance from the selected switching frequency from affecting the THD calculation.

Standards which are used to compare each scenario include *IEEE 519* [5] and SMA manufacturer standards of [6]. A table is provided in each section stating the reference requirements and the outcome of the measurements for each scenario.

1. Balanced Scenario

Figure 33 illustrates the simulated output voltage spectra in a balanced load scenario. Figure 34 illustrates the output voltage spectra measured in the laboratory in a balanced load scenario. Table 7 summarizes the balanced scenario THD results for the output voltage.

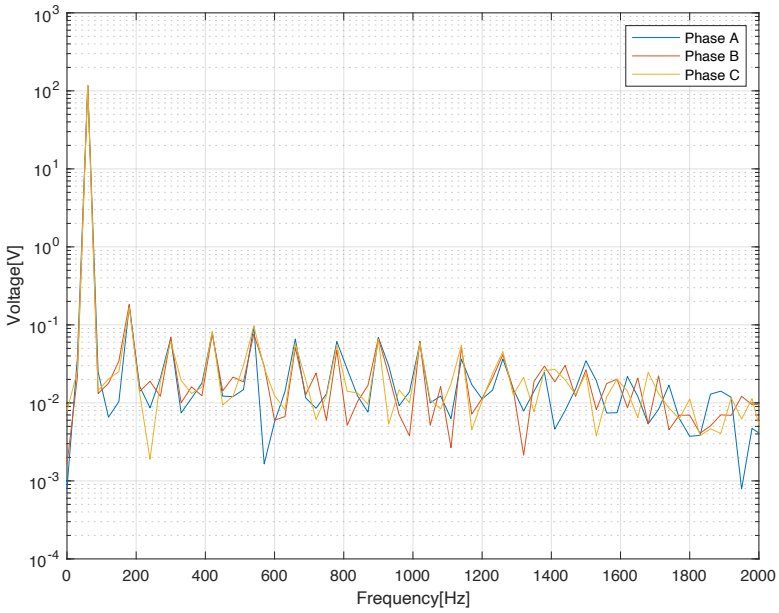

Figure 33. Simulated Output Voltage Spectra with a Balanced Load

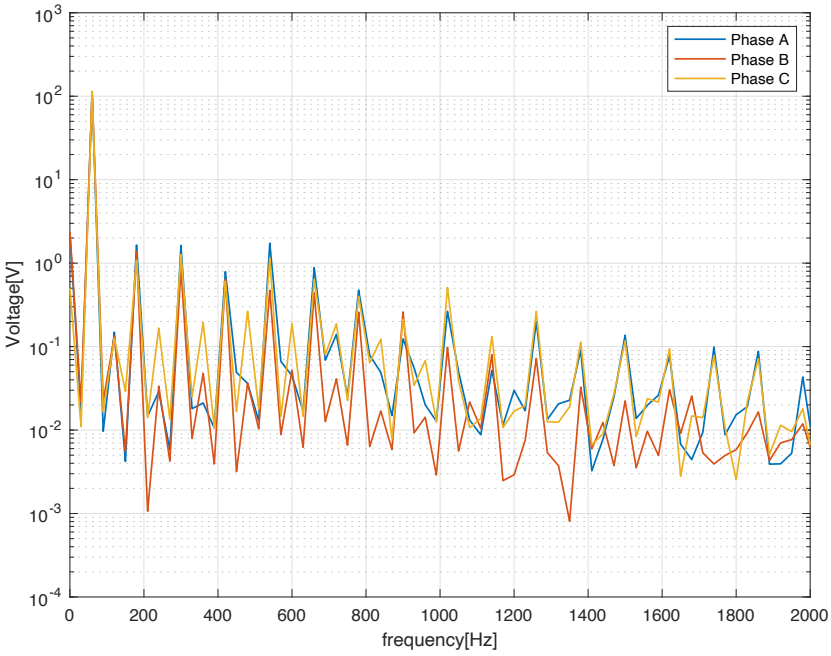

Figure 34. Experimental Measurements of the Output Voltage Spectra with a Balanced Load

Table 7. THD Balanced Load Results

	Specification Ref [5] / Mfg [6]	Model THD (%)	Laboratory THD (%)
Phase A	8% / 3%	0.5831	2.8753
Phase B		0.5779	1.6793
Phase C		0.5779	2.1143

As seen in Figures 33 and 34, the output voltage harmonics are larger in the laboratory than in the model during a balanced load scenario. Components and attributes of the model H-bridge inverter potentially affect the output voltage spectra. Specifically, the switching of the semiconductors, blanking time for switching elements, as well as isolation transformer saturation and inductive leakage. In the physics-based model, operation of the switches in the inverter are considered ideal with no blanking time present. This blanking time is the time in between switch closures which prevents a short to ground. In addition, part of this elevated response may be attributed to operations inside the COTS inverter that were unknown at the time of writing this thesis. Also, of note, distinct inter-harmonics are present, whereas in the model, they are not.

2. Unbalanced Scenario

Figure 35 illustrates the harmonic response of the model in an unbalanced load scenario. Figure 36 illustrates the harmonic response of the laboratory in an unbalanced load scenario. Table 8 summarizes the unbalanced scenario results. In this scenario, the simulated results depicted in Figure 35 show an amplified third harmonic at 180 Hz, contributing to the increase in THD. The laboratory demonstrates a reduced harmonic response on the leg with an elevated load, which is not present in the model simulation.

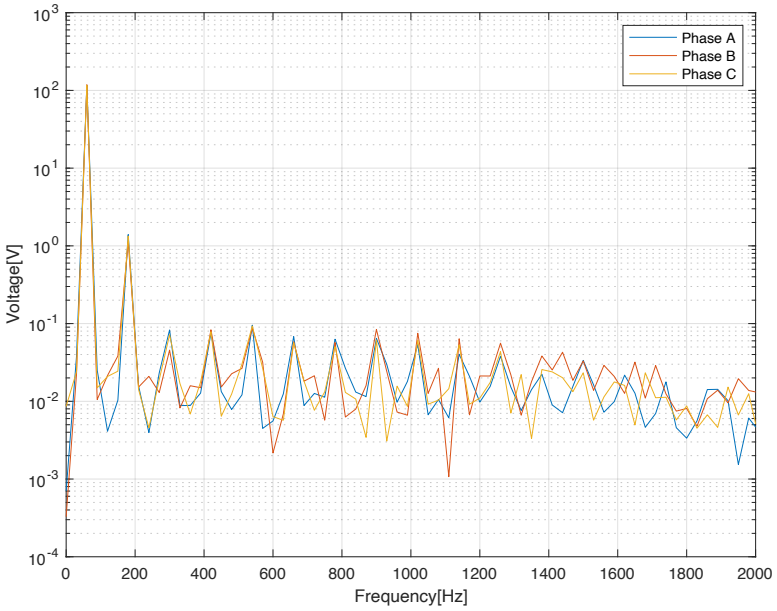

Figure 35. Model Output Voltage Spectra with an Unbalanced Load

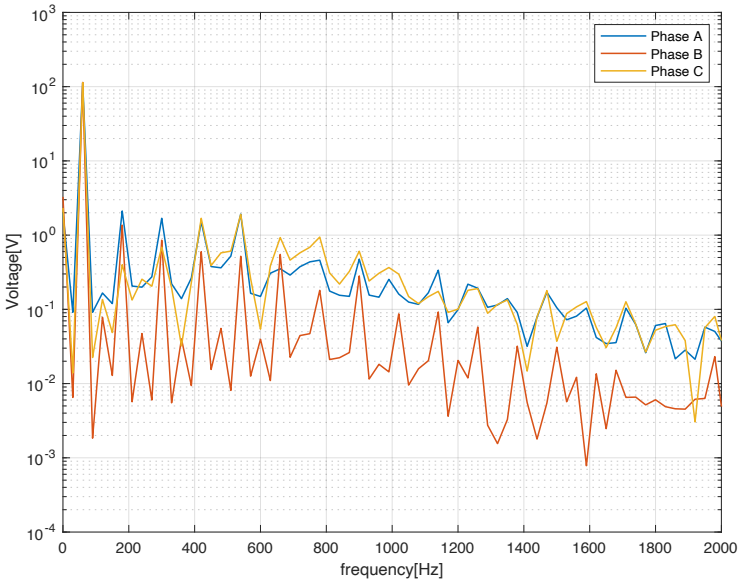

Figure 36. Experimental Measurements of the Output Voltage Spectra with an Unbalanced Load

Table 8. THD Results for the Unbalanced Load Scenario

	Specification Ref [5] / Mfg [6]	Model THD (%)	Laboratory THD (%)
Phase A	8% / 3%	1.3134	3.3705
Phase B		1.3617	1.6763
Phase C		1.3836	2.7111

C. TIME-DOMAIN VOLTAGE WAVEFORMS

1. Balanced Scenario

Figure 37 illustrates the simulated output voltage in a balanced load scenario. Figure 38 illustrates the experimental measurements of output voltage in the laboratory in a balanced load scenario. Output voltage waveforms for both laboratory and model show the presence harmonics on top of the fundamental, 60Hz, voltage components. In the simulated waveforms the high frequency ripple is the dominant characteristic. In the laboratory waveforms, the low frequency harmonics are responsible for the notching visible in the time domain. These results are consistent with the harmonic (THD) analysis presented in the previous section.

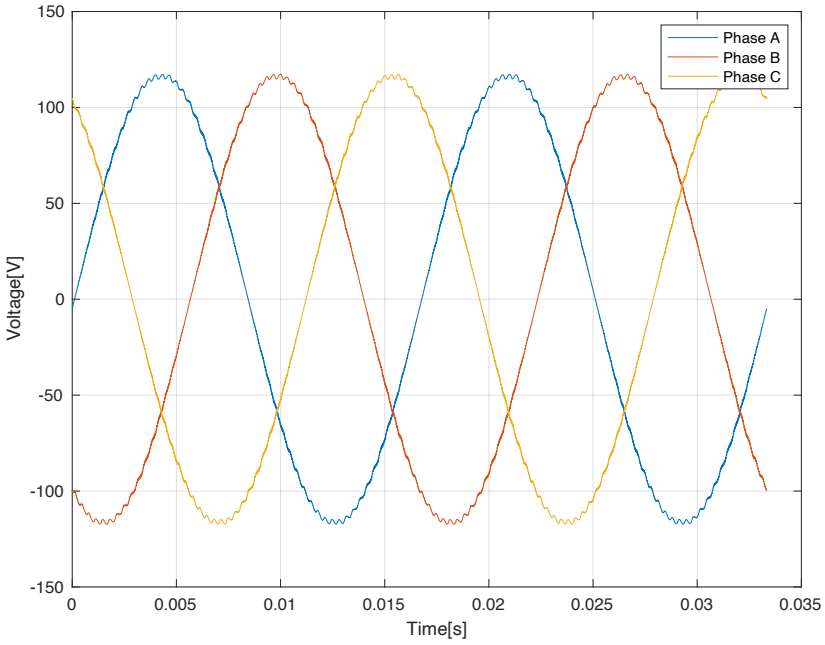

Figure 37. Simulated ac Output Voltage Waveforms with a Balanced Load

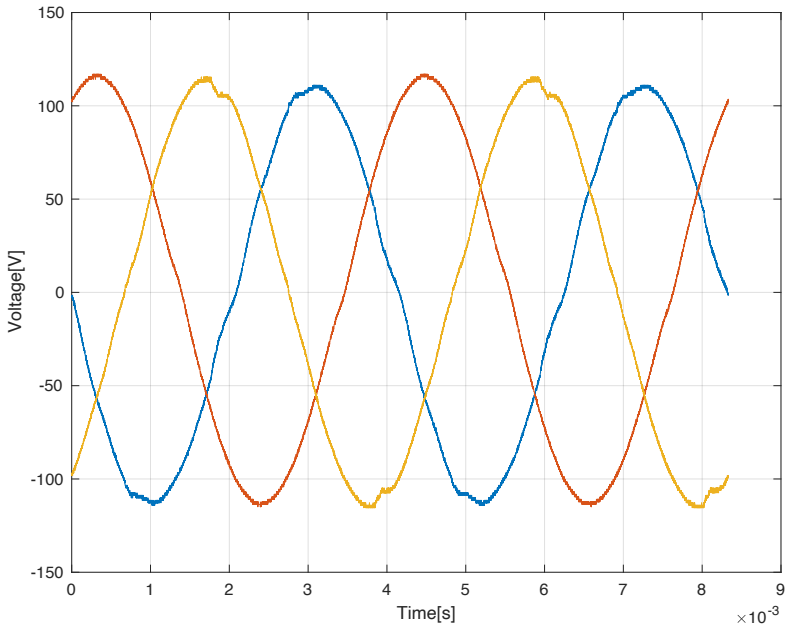

Figure 38. Experimental Measurements of the ac Output Voltage Waveforms with a Balanced Load

2. Unbalanced Scenario

Figure 39 illustrates the output voltage of the model in an unbalanced load scenario. Figure 40 illustrates the output voltage measured in the laboratory in an unbalanced load scenario.

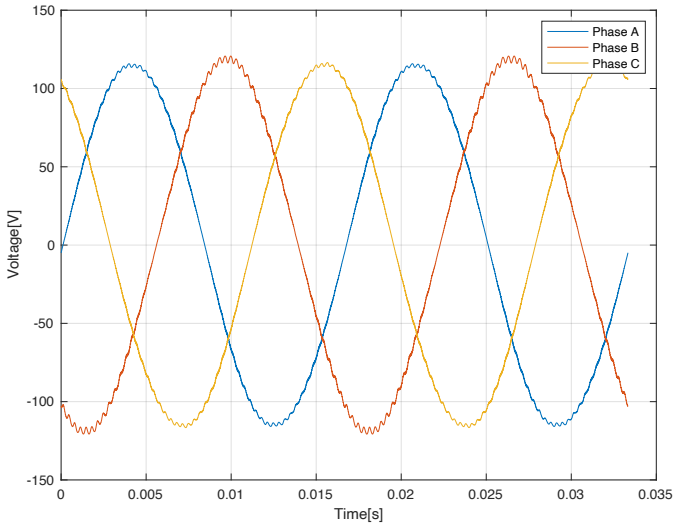

Figure 39. Simulated ac Output Voltage Waveform with an Unbalanced Load

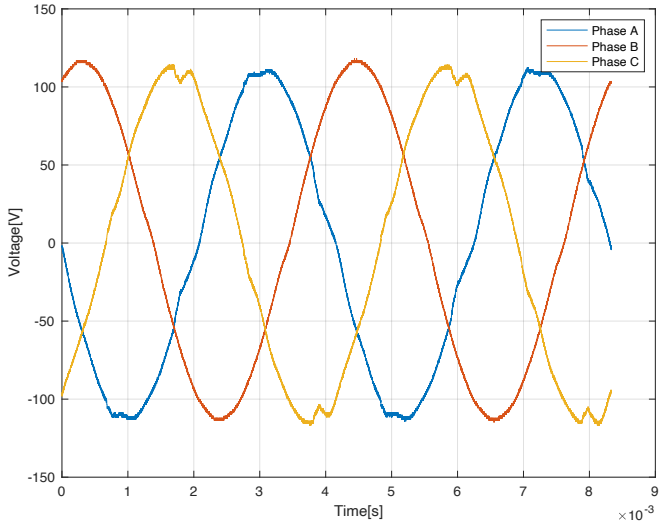

Figure 40. Experimental Measurements ac Output Waveforms with an Unbalanced Load

Both laboratory and model show the presence of harmonics on top of the fundamental, 60Hz, voltage components in both the balanced and unbalanced scenario. Again, in the simulated waveforms the high frequency ripple is the dominant characteristic. In the laboratory waveforms, the low frequency harmonics are responsible for the notching visible in the time domain. The model does not accurately develop the low frequency harmonics and their source is unknown. These results are consistent with the harmonic (THD) analysis presented in the previous section. In both scenarios, voltage amplitude differences average less than 1%.

D. LOAD CURRENTS

The method of distortion measurement in system current is referred to as Total Demand Distortion (TDD) and is omitted in this analysis. This analysis focuses on the ability of the model to accurately predict load current drawn by the load in specified loading scenarios. The loading scenarios in this analysis were limited to steady state and further evaluation of dynamic loading scenarios is required.

1. Balanced Scenario

Figure 41 illustrates the simulated load current in a balanced scenario. Figure 42 illustrates the load current measured in the laboratory in a balanced load scenario. As seen in both figures, there remains a minimal current on the neutral line. This may indicate a very slight imbalance which could be attributed to varying resistance values due manufacturing, temperature differences, or the presence of other line resistances not accounted for. Low frequency notching can be seen in the experimental measurements which is consistent with the findings in the previous two sections.

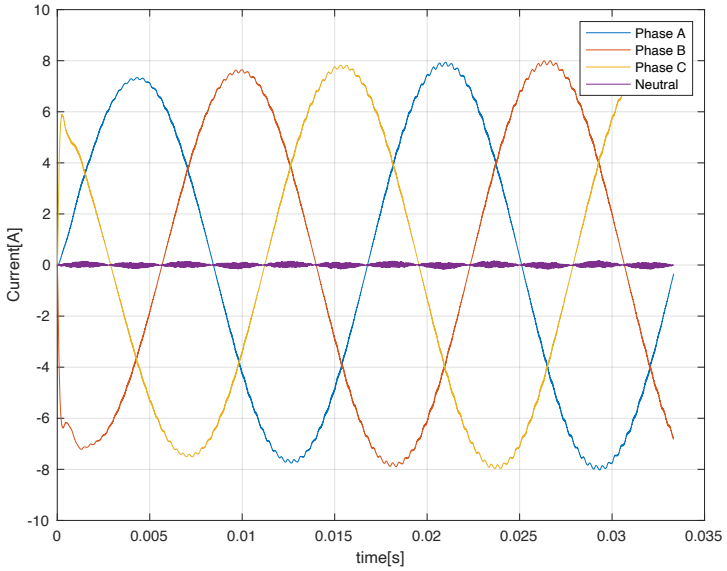

Figure 41. Simulated Load Current Waveforms with a Balanced Load

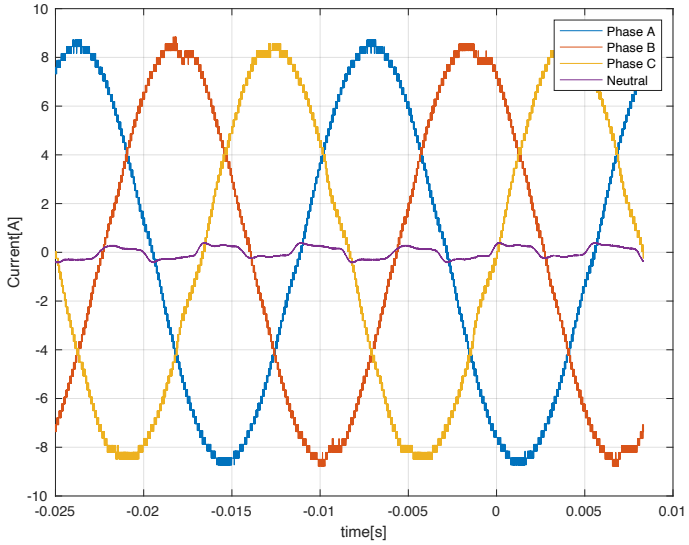

Figure 42. Experimental Measurements of Load Current Waveforms with a Balanced Load

2. Unbalanced Scenario

Figure 43 illustrates the load current of the model in an unbalanced scenario. Figure 44 illustrates the load current of the laboratory in an unbalanced scenario.

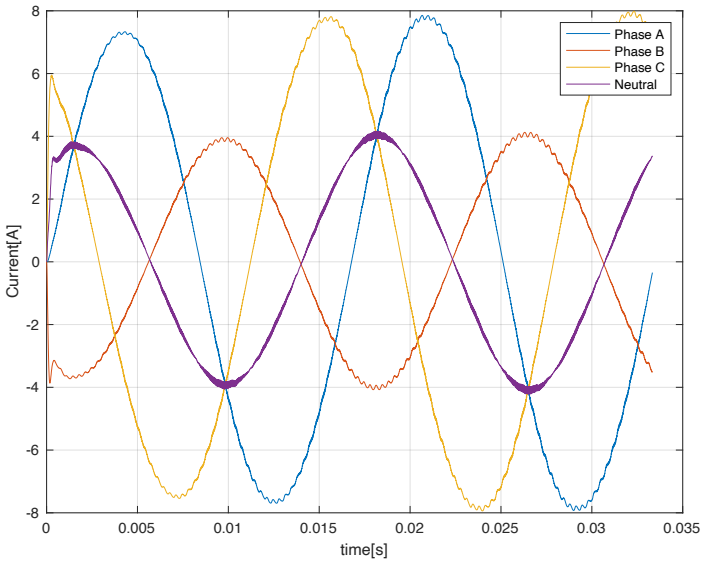

Figure 43. Simulated Load Current Waveforms with an Unbalanced Load

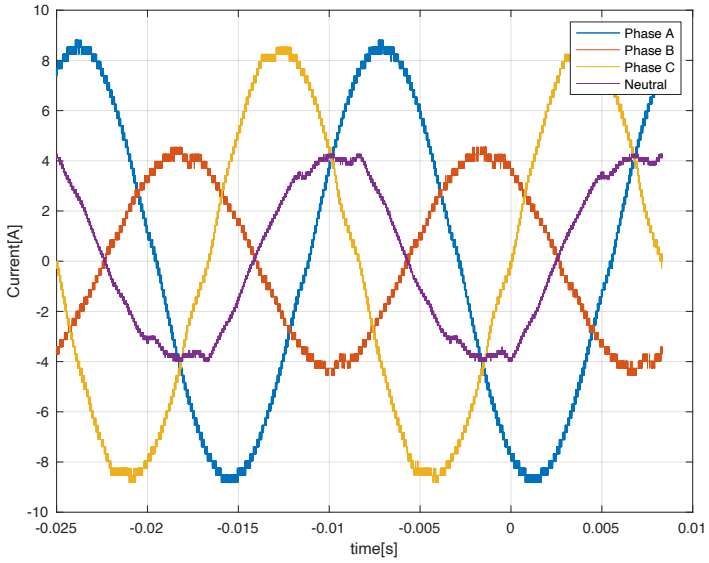

Figure 44. Experimental Measurements of the Laboratory Load Current Waveforms with an Unbalanced Load

The balanced load scenario in figures 41 and 42 indicate a small amount of neutral line current. This effect is more pronounced in the laboratory and indicates a slightly unbalanced loading of the microgrid system. In both the balanced and imbalanced load

scenarios, current waveforms demonstrate waveform distortion from both high and low frequency sources. This is congruent with the findings of the previous sections. In addition to neutral line current, the magnitude of the model load current waveform is approximately 3%-5% less than the laboratory results. This slight variance may be caused by differences in load resistance values and slight output voltage differences.

E. SUMMARY OF RESULTS

1. THD

In all scenarios, the model THD was well within both the [5] specification as well as the manufacturer specification in [6]. Table 9 summarizes all THD results.

Table 9. Summary of the THD Measurements

Scenario: Balanced				
Phase	Specification Ref [5] / Mfg [6]	Model THD%	Lab THD%	Figures
$THD_V\ \theta_A$	8% / 3%	0.5831	2.8681	33 34
$THD_V\ \theta_B$		0.5779	1.6725	
$THD_V\ \theta_C$		0.5779	2.0686	
Scenario: Unbalanced				
Phase	Specification Ref [5] / Mfg [6]	Model THD %	Lab THD%	Figures
$THD_V\ \theta_A$	8% / 3%	1.3134	3.3705	35 36
$THD_V\ \theta_B$		1.3617	1.6763	
$THD_V\ \theta_C$		1.3836	2.7111	

2. Voltage

Root-mean-square voltage measurements and predictions were accurate within 1% for both balanced and unbalanced scenarios.

3. Current

Root-mean-square current measurements and predictions were accurate within 5% for both balanced and unbalanced scenarios.

THIS PAGE INTENTIONALLY LEFT BLANK

VI. CONCLUSION AND FUTURE WORK

A. CONCLUSION

A physics-based model of a three-phase microgrid assembled in the NPS laboratory using COTS converters was designed and implemented in *Simulink* [7] for two different scenarios. The goal was to generate a model that represents the laboratory set-up so that it can be used for future research, such as development of novel energy management strategies, control systems and extension of the laboratory microgrid. Time-domain waveforms as well as spectra and THD were simulated and compared to the experimental waveforms measured in the laboratory. Based on a model generalization, all output filters of the H-bridge converters were assumed to be perfectly matched. In the real-world components, this would not be true and would potentially lead to minimal output differences between phases. There were limitations on matching THD of the model to the laboratory results due to the unknown configuration and operation of the COTS converters.

Other factors effecting the accuracy of the model include the use of an ideal switching scheme for the operation of the inverter. Voltage losses across the switching transistors and blanking time between switch operations was omitted, enhancing the performance of the inverter. In addition, an ideal transformer was used at the output of the inverter thereby neglecting inductive losses and saturation effects.

Output voltage and load current time-domain waveforms were accurately modeled when compared to the laboratory measurements. Specifically, currents were within 5% of the real-world laboratory performance on a highly accurate resistive load.

Measurement of the actual converter units and model performance indicate that based on THD, the Sunny Island converters conform to the manufacturer specification in the balanced mode of operation. In an unbalanced mode of operation, results indicate that some phases exceed the manufacturer specification of 3%. This variance is not seen in the model. In addition, the COTS converters conform to [5] standards.

Further refinement of the converter model, as noted in future work, will help produce a more realistic operational performance. Without the inner workings of the COTS system, the converters could only be functionally represented in the model.

B. FUTURE WORK

1. Model Refinement

The model developed for this evaluation represents ideal conditions and assumed processes for developing the providing power to the load. More research and collaboration with the manufacturer of the SMA Sunny Island converters is necessary to refine this model real-world performance. Some of these processes may be proprietary which will prevent the most accurate development of this model.

2. More Load Scenarios

Evaluation of the modeled microgrid should include other DERs, grid-tied scenarios, generator use, and dynamic loading scenarios. In addition to steady state scenarios, other scenarios providing analysis of transient response would be beneficial. Characterizing the normal operation of deployed microgrids will provide a robust recommendation for the use of these and other commercial units.

APPENDIX A. LABORATORY SETUP INSTRUCTIONS

EQUIPMENT REQUIRED
FLUKE 434/435 Power Meter
3 High Voltage Differential Probes
4 Pearsons Current Monitors
3 Phase Load
4 Channel Oscilloscope with USB port
6 8–12 AWG wires which will connect to the High Voltage Differential Probes with stripped ends to install in the breaker panel.
4 2–4 AWG wires to connect the load to the breaker panel
2 Power strips
1 Extension cord
FLUKE multimeter

COMPUTER SETUP
This configuration uses MATLAB as a battery state of charge (SOC) monitor. There are also indications on the front of the Sunny Island inverters. The program is run periodically during testing to ensure that the minimum SOC of 85% is not reached. If this level is reached, testing should be suspended until other distributed energy resources recharge the batteries. Appendix C has the code for this monitoring.
*There is no internet at the lab. Most likely the MATLAB program will need to be updated or re-registered. This can be accomplished in the offices at the golf course or back at NPS. ITACS can do the update if there is sufficient time.

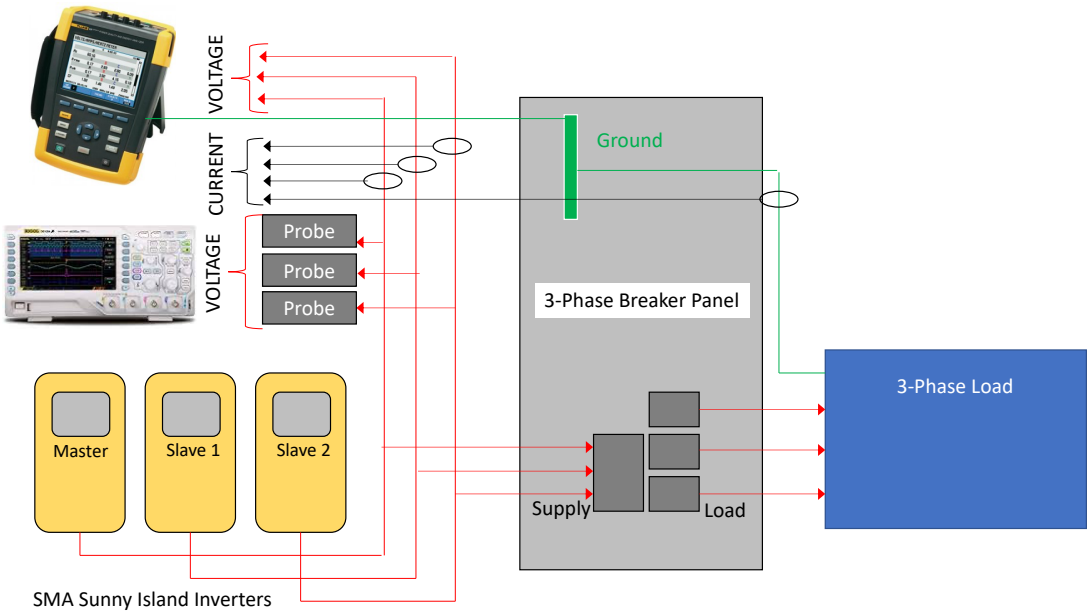

CONNECT LOAD

1. Shutdown the Sunny Island Inverters from Right to Left (Slave 2, Slave 1, Master)
2. Open panel supply breaker
3. Check that the panel dead
4. Open 3 breakers to the heater load
5. Remove heater load wires from heater breakers. There will be two wires per breaker. These will be the breakers to connect the loads to.

*Note heater load wires are labeled with 3 different colors to help reinstall when finished.

6. Connect neutral/ground from load to ground bus bar in the upper left of the breaker panel. This is where all the breaker panel WHITE wires are connected.
7. Run 3 leads from each phase of the load to the load breakers in the bottom right hand side of the breaker panel. Prior to energizing, check the resistance of each phase with a multimeter.
8. Have a 120 Vac plugin handy to plug in the cooling fan of the three-phase resistor load.

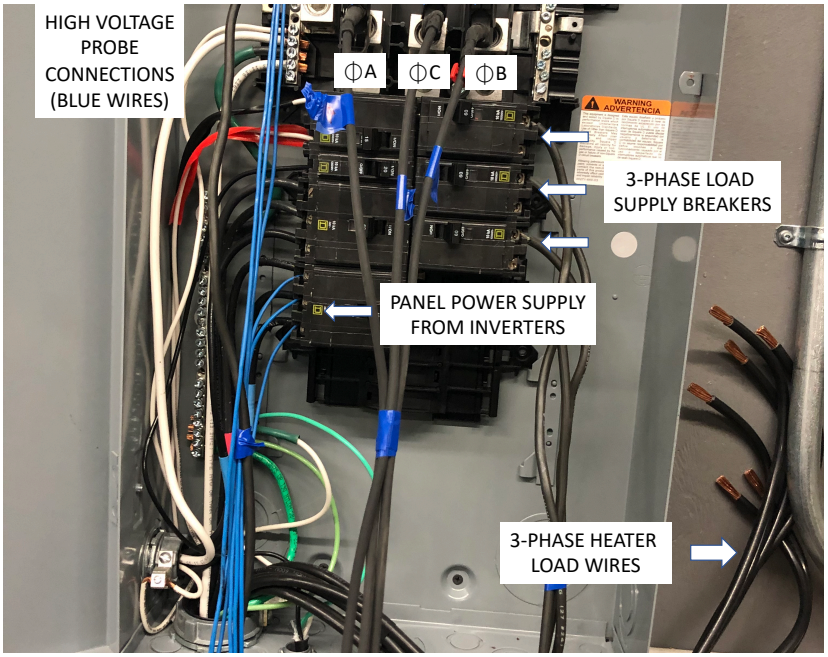

CONNECT FLUKE

*There is not a data collection method from the FLUKE that will produce waveforms for voltage or current which are transferrable to MATLAB. Plots can be displayed on the computer, but will not assist in displaying data in MATLAB. The FLUKE is best used to validate findings for voltage waveforms, power, total harmonic distortion, etc.

1. Set up fluke location and get 4 wire clamps (current) and 4 alligator connectors.
2. Connect the ground/neutral to the ground of the load or the breaker panel ground bus bar.
3. Install 3 alligator connectors to the main 3 bus bars located at the top of the breaker panel. Phase sequence of the panel is A-C-B from left to right.
4. Connect 4 current clamps to FLUKE and place them on each phase including neutral.

*Note orientation of current clamps for direction of current flow. The indication is imprinted on each clamp.

CONNECT OSCILLOSCOPE

*Need an oscilloscope that has 4 channels in order to simultaneously monitor and collect data on phases A-C and ground/neutral. In this configuration, with only one oscilloscope, either voltage or current can be monitored, not both.

1. Connect 3 8–12AWG wires from the breaker panel neutral bus bar. These are connected to the ground of the High Voltage Differential Probes.
2. On the breaker panel SUPPLY breaker, located in the lower left-hand side of the panel, install one 2–4 AWG wire in each phase of the supply breaker, leaving the existing supply wire installed.
3. Connect grounds and supply leads to each High Voltage Differential Probe. Plug in the High Voltage Differential Probe and verify power by the green light indication. If no green light shows, shift the power supply. Note the position of the grey button for scaling, it should be depressed
4. The ground/neutral line does not need an High Voltage Differential Probe.
5. Slide the current clamps over each phase, A-C, and ground/neutral.

*Note there is a scaling factor associated with each current clamp. This must be accounted for in MATLAB after data collection.

*NOTE: It was helpful to group the current wires together and the voltage wires together with tape, with each phase labeled.

POWER UP AND TEST CONNECTIONS

*Recommend powering up the FLUKE first and once proper operation is verified, then power up the oscilloscope.

WARNING: Make sure the High Voltage Differential Probes are powered on prior to turning on the oscilloscope. The high voltage could damage it.

1. Close the Sunny Island inverter switches one at a time, starting with the Master on the left, and working to the right.
2. Check voltage at the supply breaker leads with multimeter.
3. Close the supply breaker.
4. At this point the FLUKE should have voltage indications and phase sequence can be checked. If a discrepancy is found, relocate the phase lines to the oscilloscope to match.
5. Plug in the resistor load cooling fan.
6. Shut the load breakers.
7. The FLUKE Power Meter should now have indications and plots for power, current, and THD.
8. Open the load breakers and turn off the cooling fan.

*Minimizing the time the load is energized will ensure that the minimum battery SOC of 85% is not reached.

9. Verify High Voltage Differential Probes are powered on.
10. Turn on the oscilloscope. Connect the leads for voltage monitoring. Verify the incoming voltage waveforms and phase sequence. Note the scale of the High Voltage Differential Probes prior to collecting data in order to scale the data properly in MATLAB.

11. Test the data collection method applicable to the oscilloscope selected.
12. Remove the voltage leads and plug in the current clamp leads.
13. Plug in the load cooling fan and close the load breakers. Verify sequence and magnitude using the current waveforms with the applicable scaling factor.

SHUTDOWN

1. Ensure the load breakers are open.
2. Open the supply breaker.
3. Ensure that the Sunny Island inverters remain ON so that they may charge the batteries.

APPENDIX B. SIMULINK MODEL

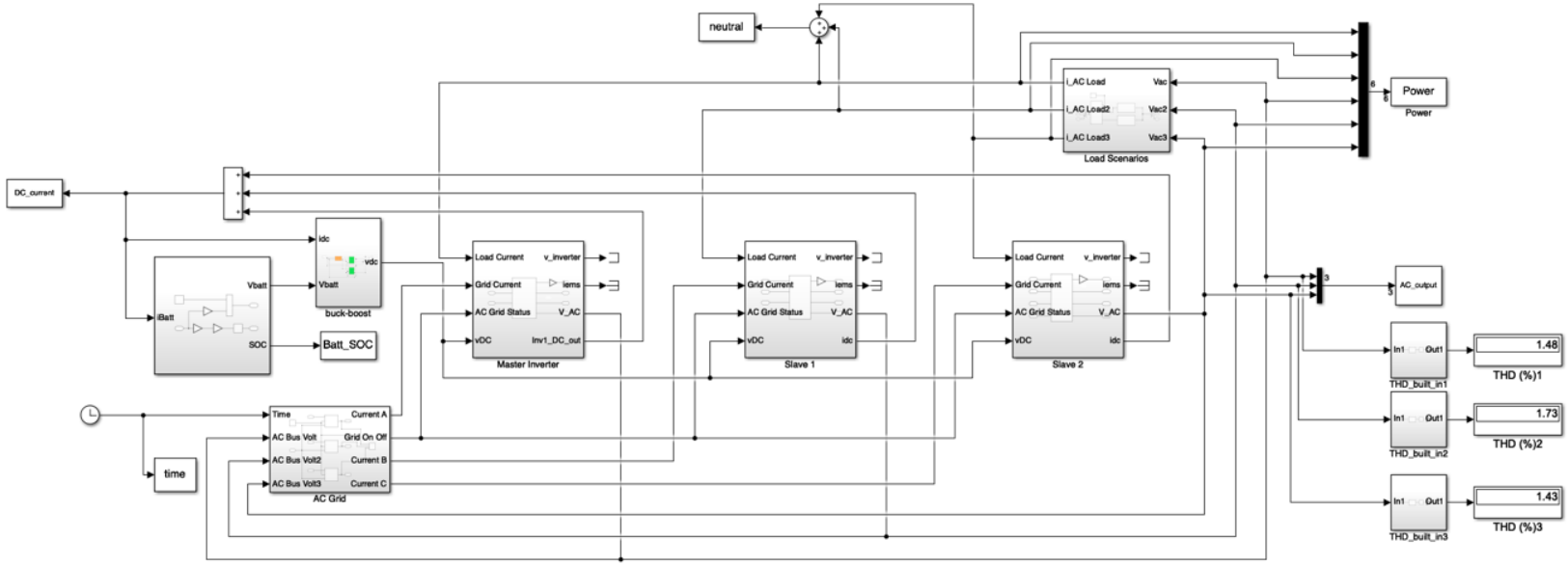

THIS PAGE INTENTIONALLY LEFT BLANK

LIST OF REFERENCES

[1] *IEEE Standard for Interconnection and Interoperability of Distributed Energy Resources with Associated Electric Power Systems Interfaces,* IEEE Std 1547–2018, February 15, 2018.

[2] *IEEE Powering and Grounding Electronic Equipment,* IEEE Std 1100–2005, December 29, 2009.

[3] *IEEE Recommended Practice for Monitoring Electric Power Quality,* IEEE Std 1159–2019, June 13, 2019.

[4] N. Mohan, T.M. Underland, and W.P. Robbins, *Power Electronics: Converters, Applications, and Design.* Hoboken, NJ, USA: John Wiley and Sons, 2003.

[5] *IEEE Recommended Practice and Requirements for Harmonic Control in Electric Power Systems*, IEEE Std 519–2014, March 27 2014.

[6] SMA Solar Technology America LLC, "*Off-Grid Inverter Sunny Island 4548-US/ 6048 U.S. Operating Manual*," SI4548-6048-US-BE-en-21, Version 2.1, 2015. [Online]. Available: https://files.sma.de/dl/15216/SI4548-6048-US-BE-en-21W.pdf

[7] Simulink by Mathworks (2020, Jan.). [Online] Available: https://www.mathworks.com/products/simulink.html

[8] D. Kanavaros, "Implementation of active and reactive power flow control in a single phase microgrid," M.S. thesis, Elect. Comput. Eng., Naval Postgraduate School, Monterey CA, USA, 2019.

[9] A. Werth, N. Kitamura, I. Matsumoto, K. Tanaka, "Evaluation of centralized and distributed microgrid topologies and comparison to Open Energy Systems," *ResearchGate,* Jul. 2015. [Online]. doi: 10.1109/EEEIC.2015.7165211

[10] W. Jing, C. Hung Lai, S. H. W. Wong, and M. L. D. Wong, "Battery-supercapacitor hybrid energy storage system in standalone DC microgrids: a review," *IET Renew. Power Gener.*, vol. 11, no. 4, pp. 461–469, Mar. 2017. [Online]. https://doi.org/10.1049/iet-rpg.2016.0500.

[11] Y. V. P. Kumar and R. Bhimasingu, "Performance analysis of green microgrid architectures by comparing power quality indices," *Eighteenth National Power Systems Conference (NPSC)*, Guwahati, India, 2014, pp. 1–6, 2014. [Online]. https://doi.org/10.1109/NPSC.2014.7103873.

[12] K. Hawxhurst. "Microgrid control strategy utilizing thermal energy storage with renewable solar and wind power generation," M.S. thesis, Elect. Comput. Eng., Naval Postgraduate School, Monterey CA, USA, 2016.

[13] G. Oriti, A. L. Julian, and N. J. Peck, "Power-Electronics-Based Energy Management System With Storage," IEEE Trans. Power Electron., vol. 31, no. 1, pp. 452–460, Jan. 2016, doi: 10.1109/TPEL.2015.2407693.

[14] “Pulse-width modulation.” *Wikipedia*. Accessed 8 Feb. 2020. [Online] Available at: https://en.wikipedia.org/wiki/Pulse-width_modulation

[15] GW Energy. (2020). PFC Graphs. Accessed 7 Feb. 2020 [Online] Available at: https://gwenergy.co.uk/pfc-graphs/

INITIAL DISTRIBUTION LIST

1. Defense Technical Information Center
   Ft. Belvoir, Virginia

2. Dudley Knox Library
   Naval Postgraduate School
   Monterey, California